(12)

AD A131528

Multifrequency HF radar observations of currents and current shears

Calvin C. Teague
Stanford Center for Radar Astronomy
Stanford University

DTIC FILE COPY

July 1983

DTIC
ELECTE
AUG 1 8 1983
S D
A

Final Report, ONR Contract N00014-75-C-0356

Accession For
Letter on file
DTIC COPY INSPECTED
A

This document has been approved for public release and sale; its distribution is unlimited.

83 07 29 005

Abstract

During the period of January 1975 to January 1982, techniques were developed for using high-frequency (HF: 3–30 MHz) radar to measure ocean currents and vertical current shears in the upper one or two metres of the ocean surface. The measurement of current velocity with an HF radar depends on the ability of the radar to precisely measure the phase velocity and direction of propagation of ocean waves whose wavelength is one-half the radar wavelength. In the absence of a current, the waves travel at a speed given by the still-water dispersion relation. An underlying current will modify this speed. The radar measures the actual phase velocity through a Doppler shift, and the wavelength of the ocean wave is known through the first-order Bragg scattering relation, so a difference between observed and theoretical still-water phase velocity can be calculated. In addition, longer ocean waves are affected by currents at deeper depths than are shorter ocean waves. By measuring the phase velocity at several different wavelengths, it is possible to measure a vertical current shear in the top one or two metres of the ocean surface. This is a measurement that is very difficult to make by any other means.

A portable coherent, pulsed-Doppler HF radar system was developed ~~at Stanford~~ and used in several experiments, both on land on the California coast and on board a ship during the JASIN experiment. Two different antenna systems were developed during the course of the experiments. The land-based experiments used a balloon-supported vertical half-rhombic transmitting antenna and a single wideband receiving loop. The shipborne experiment used a multi-element omnidirectional transmitting antenna with a steerable phased array consisting of eight wideband loops for the receiver.

Land-based experiments conducted at Pescadero, California demonstrated that a current could be measured by an HF radar, and that its value agreed well with that measured by *in-situ* drifting spar buoys. In addition, there was evidence of a vertical current shear, both from the radar measurements and from the buoy measurements. The equipment and data processing techiques were developed during the Pescadero

experiments.

The JASIN experiment was an attempt to apply these techniques to the measurement of surface current and current shear in the open ocean. The radar system was successfully installed on board a ship with tolerable interference to the other shipboard activities. The steerable antenna was quite rugged and performed as expected. It produced antenna patterns consistent with the physical aperture of the array. The wind velocity during the JASIN experiment was quite low, so wind- and wave-generated currents were quite small. Nevertheless, there is some evidence of a current shear. Its magnitude is small and near the resolution limit of the radar, but it appears to be about 50% higher than what would be expected from the wind and wave conditions present at the time of the experiments.

Contents

Page

Chapter 1. Introduction 1

Chapter 2. Theory 3

2.1 First-order radar scattering 3

2.2 Vertical current shear 4

2.3 Wind-induced shear 5

2.4 Wave-induced shear 6

Chapter 3. HF radar system 8

3.1 Transmitter 8

3.2 Receiver 10

3.3 Data sampling and recording 10

Chapter 4. The Pescadero Experiments 12

4.1 Radar installation 12

4.2 Spar buoys 15

4.3 Data processing 18

4.4 Results 20

Chapter 5. The JASIN Experiment 24

5.1 Radar installation 24

5.2 Data processing 30

5.2.1 Estimating the current 30

5.2.2 Estimating the ocean-wave directional spectrum 39

5.3 Results 41

Chapter 6. Summary and Conclusions 46

References 48

Acknowledgements

Robert Stewart of the Scripps Institution of Oceanogaphy has worked very closely with Stanford throughout the entire HF radar ocean-wave backscatter research program. The analysis of the data from the Pescadero experiments was performed by Eng Chong Ha, and the work leading to his dissertation provided the basis for our participation in the JASIN experiment. The JASIN experiment described here required the cooperation of the officers and crew of the R. V. *Atlantis-II*, operated by the Woods Hole Oceanographic Institution, and the West German R. V. *Meteor*. The JASIN experiment was coordinated by the British Royal Society. Several individuals at Stanford including Taylor Howard, Kent Price, Abid Elabdalla, Frank Orabona, and Bill Crosby provided invaluable assistance. This work was performed under ONR contract N00014-75-C-0356.

Chapter 1

Introduction

This report covers the period January 1975 to January 1982. The aim of the research described here was to develop techniques for using high-frequency (HF: 3–30 MHz) radar to measure ocean currents and vertical current shears in the upper one or two metres of the ocean surface. Some of the research was conducted using land-based equipment (at a site on the California coast near Pescadero), and some was conducted from a shipborne platform (the R.V. *Atlantis II* during the Joint Air-Sea Interaction Experiment – JASIN). The radar equipment, specially developed at Stanford for this research, was the same in both cases, but the antenna systems differed widely between the two experiments.

The measurement of current velocity with an HF radar depends on the ability of the radar to precisely measure the phase velocity and direction of propagation of ocean waves whose wavelength is one-half the radar wavelength. This is first-order scattering [*Barrick*, 1972a], and in contrast to second-order scattering [*Barrick*, 1971, 1972b], which involves two or more ocean wave trains often travelling in different directions, the first-order lines are usually very sharp, often only a few millihertz wide at a radar carrier frequency of several megahertz. The Bragg scattering mechanism has been well established as responsible for first-order echoes [*Crombie*, 1955, *Barrick*, 1972a]. Thus it is possible to relate the phase velocity of the ocean waves, as determined by the Doppler shift of the radar echoes, to the wavelength of the ocean waves, as determined by the wavelength of the radar signal. The difference between the observed phase velocity of

the ocean waves and its value predicted by the deep-water dispersion relation has been attributed to surface currents [*Stewart and Joy*, 1974]. Furthermore, this difference often is a function of ocean (or radar) wavelength, and this is attributed to a vertical current shear, since longer wavelength ocean waves are influenced by currents at deeper depths than are shorter ocean waves. It is this wavelength dependence which suggests that an HF radar can be used to measure a vertical current shear.

The first-order scattering mechanism is highly selective in terms of the direction of wave propagation: only those ocean waves which are travelling radially toward or away from the radar contribute appreciable energy to the first-order echo. Consequently, ocean-wave directional resolution is obtained by radar antenna directivity. Other techniques, such as those used by the CODAR, [*Barrick, Evans and Weber*, 1977] can provide high directional resolution with smaller antennas than those used here, but they were not employed because of the need to operate over a wide range of radar frequencies in order to measure a vertical current shear.

Early observations were carried out by *Stewart and Joy* [1974], who showed that surface currents could be measured by an HF radar system. More importantly, they demonstrated that the observed current was a function of radar wavelength, implying that a vertical current shear could be measured by HF radar. To determine the accuracy of the technique, and to extend these early observations, we conducted a series of experiments at Pescadero, California, and we participated in the JASIN experiment. The same HF radar system was used in both experiments, but with different antenna systems. In both experiments, the Scripps pitch-roll buoy [*Stewart*, 1977] was used to measure the directional ocean-wave spectrum. These experiments were conducted jointly by Stanford University and Scripps Institution of Oceanography.

Chapter 2

Theory

2.1 First-order radar scattering

Crombie [1955] first made the observation that radio signals scattered by the ocean surface consisted of a pair of very narrow sidebands displaced above and below the carrier frequency by a small amount (a fraction of a Hz at HF). This frequency corresponded exactly to the Doppler shift of an object moving at the phase velocity of an ocean wave whose wavelength was one-half the radio wavelength. He deduced that the scattering mechanism was Bragg scattering, in which the contributions from each individual wave crest all add up coherently to produce the scattered signal. *Hasselmann* [1966] showed that a vertically-polarized radio wave propagating at grazing incidence, with a wavenumber $\mathbf{k}_i$ and frequency ω_i is scattered into two waves of wavenumber $\mathbf{k}_s$ and ω_s such that

$$\begin{aligned} \mathbf{k}_s &= \mathbf{k}_i \pm \mathbf{k} \\ \omega_D &= \omega_s - \omega_i = \pm\omega \end{aligned} \tag{1}$$

where ω_D is the Doppler shift of the scattered radio wave and $\mathbf{k}$ and ω are the wavenumber and frequency of the ocean surface wave. For the case of backscatter (co-located transmitter and receiver) $\mathbf{k}_s = -\mathbf{k}_i$, so that $2\mathbf{k}_s = \pm\mathbf{k}$. *Barrick* [1972b] examined the scattering mechanism in more detail and extended the geometry to include non-grazing incidence.

The ocean-wave velocity c depends on an underlying current. Let the still-water wave velocity be c_1 and the velocity in the presence of a current be c_p. By definition, $c_p = \omega_p/k$ and $c_1 = \omega/k$. Their difference v is

$$v = k^{-1}(\omega_p - \omega) = k^{-1}\Delta\omega \tag{2}$$

where $\Delta\omega$ is the difference between the observed Doppler shift and its expected value. The dependence of v on the vertical current distribution is discussed in the next section. *Stewart and Joy* [1974] discuss this theory in more detail.

When the ocean surface roughness is calculated to second order, it is found that the Bragg line itself has sidebands. *Barrick* [1971] showed that this continuum depends on all of the ocean waves present, not just the Bragg component, and *Hasselmann* [1971] suggested that this can be used to measure the entire ocean-wave spectrum using a single radio wavelength. However, the presence of the second-order sidebands does not alter the position of the first-order line, so as long as its position can be accurately determined, the second-order continuum does not affect the current measurement capability of the radar system. Only the first-order line will be used in the remainder of this report.

2.2 Vertical current shear

The relationship between radar wavelength and the effective depth of the current measurement was first examined by *Stewart and Joy* and has recently been examined by *Ha* [1979] as part of a Ph.D. dissertation at Stanford University. The difference in velocity between a wave in a current field and one in still water is

$$U(k) = 4k\int_0^\infty u_k(z)\exp(-4kz)\,dz \tag{3}$$

where $u_k(z)$ is the component of the horizontal current in the direction of the radar beam at depth z, and $k = \pi/L$ is the radio wavenumber for a radar in resonance with ocean waves of length L. If the current profile is logarithmic, that is

$$u_k(z) = u_s - \frac{u_*}{K}\ln\left(\frac{z}{z_0}\right) \tag{4}$$

where u_s is the surface drift, u_* is the friction velocity, $K = 0.4$ is Von Karman's constant, and z_0 is the reference depth, then the radar probes the logarithmic current at a depth of approximately 4.4% of the ocean wavelength [*Ha*, 1979]. If a linear profile is assumed, as was done by *Stewart and Joy*, then the current is probed at a depth of approximately 7.8% of the ocean wavelength. For example, in the JASIN experiment the ocean wavelengths were 31.2, 22.1, 11.2, and 6.9 m. For this case, if a logarithmic profile is assumed, the radar system probes the current at depths of approximately 137, 97, 49, and 30 cm, and if a linear profile is assumed, the depths are 244, 173, 88, and 54 cm, respectively. Substituting (4) into (3), and assuming $4Kz_0 \ll 1$,

$$U(k) = u_s + \frac{u_*}{K}\ln(4k\gamma z_0) \tag{5}$$

where $\gamma = 1.781072$. Differentiating,

$$\frac{dU(k)}{d\ln F} = \frac{u_*}{K} \tag{6}$$

where F is the radio frequency having ocean wavenumber k and $U(k)$ is the current velocity seen by this radio frequency [*Wu*, 1975], [*Teague et al.*, 1977].

2.3 Wind-induced shear

It is believed that the wind produces a vertical current shear, because the wind blowing over the sea drags the surface layers along in the direction of the wind, and these surface layers further influence deeper water. In order to estimate the magnitude of the wind-induced shear, it is assumed that the velocity profile in the water is logarithmic and given by (4). For flows past a free boundary, the stress τ is given by $\tau = \frac{1}{2}\rho u_*^2$, where ρ is the fluid density and u_* is the friction velocity. If it is assumed that the stress τ is constant across the air-sea boundary, then

$$\tau_{air} = \frac{1}{2}\rho_{air}u_{*air}^2 = \frac{1}{2}\rho_{water}u_{*water}^2 = \tau_{water}. \tag{7}$$

If the stress is given by $\tau = C_D \rho U^2$, where $C_D = 1.3 \times 10^{-3}$ is the drag coefficient in the air and U is the air velocity at 10 m, then

$$u_{*water} = \left(\frac{\rho_{air}}{\rho_{water}}\right)^{\frac{1}{2}} (C_D)^{\frac{1}{2}} U. \tag{8}$$

For $U = 10\ \mathrm{m\,s^{-1}}$ this would predict a current shear of $5\ \mathrm{cm\,s^{-1}}$ between the top layer and the bottom layer probed by the radar.

2.4 Wave-induced shear

The ocean surface waves also are believed to produce a vertical shear through the Stokes drift. The Stokes drift arises because a wave of finite amplitude, accompanied by irrotational fluid motion, requires that the water particle orbits are not quite closed; there is a small net mass transport in the direction of wave propagation [*Kinsman*, 1965, p. 256]. *Van Dyke* [1982, p. 110] displays some striking photographic examples of this effect. In order to estimate this drift, the vertical current profile is predicted using Stokes' theory of wave-produced currents and the pitch-roll buoy measurements of the entire set of ocean surface waves present during the radar measurements. The vertical current distribution as a function of depth z is estimated from

$$u(z) = \frac{2}{\rho g^2} \int_0^\infty F(\omega)\omega^3 \exp(-2\omega^2 z/g) d\omega \tag{9}$$

where g is the gravitational acceleration and $F(\omega)$ is the surface elevation energy density at frequency ω [*Kenyon*, 1969]. Then for each of the waves to which the radar system is sensitive, the integrated effect of this current profile on the wave phase velocity is computed by using the current distribution (9) in (3). In performing this calculation, it is assumed that the Lagrangian current produced by a wave spectrum advects a short wave, thus changing its phase velocity. This is not precisely true, but the influence of other wave interactions is small. That is, the influence of wave interactions is to produce a current which modifies the phase velocity of individual wave components;

other interactions which directly change the wave phase velocity, without producing currents, are small. The shear predicted in this manner is on the order of 1–6 $\mathrm{cm\,s^{-1}}$ over the depth probed by the radar for the wave conditions encountered in the experiments.

Chapter 3

HF radar system

The radar system used in the experiments was developed at Stanford specially for this program. It is a pulsed coherent Doppler radar which can transmit and receive pulse-interleaved signals simultaneously on four different frequencies in the range of 4–30 MHz. The exact frequencies are selectable in 10 kHz steps. The frequencies are generated by a set of phase-locked loops. The same signals are used in both the transmitter and receiver, thus minimizing the amount of hardware required and ensuring coherence between the transmitter and receiver internal signals. The radar system includes a digital sampling and recording system. The entire radar, exclusive of the power amplifier, occupies 12 inches of panel space. The power amplifier occupies another 10 inches.

3.1 Transmitter

The transmitter and receiver frequencies are generated by a set of four phase-locked loops. These each generate signals in the range of 34–60 MHz. A fifth phase-locked loop is fixed at 30 MHz. The transmit signal is obtained by mixing the signal from one of the first 4 loops with the 30 MHz signal, producing a signal in the range of 4–30 MHz. The signals from each of the four oscillators are selected, one at a time at 400 μs intervals, to provide the interleaved transmitter pulse train. The pulse widths are selectable from 10 to 200 μs. The pulse rise and fall times are controlled to minimize the ocupied

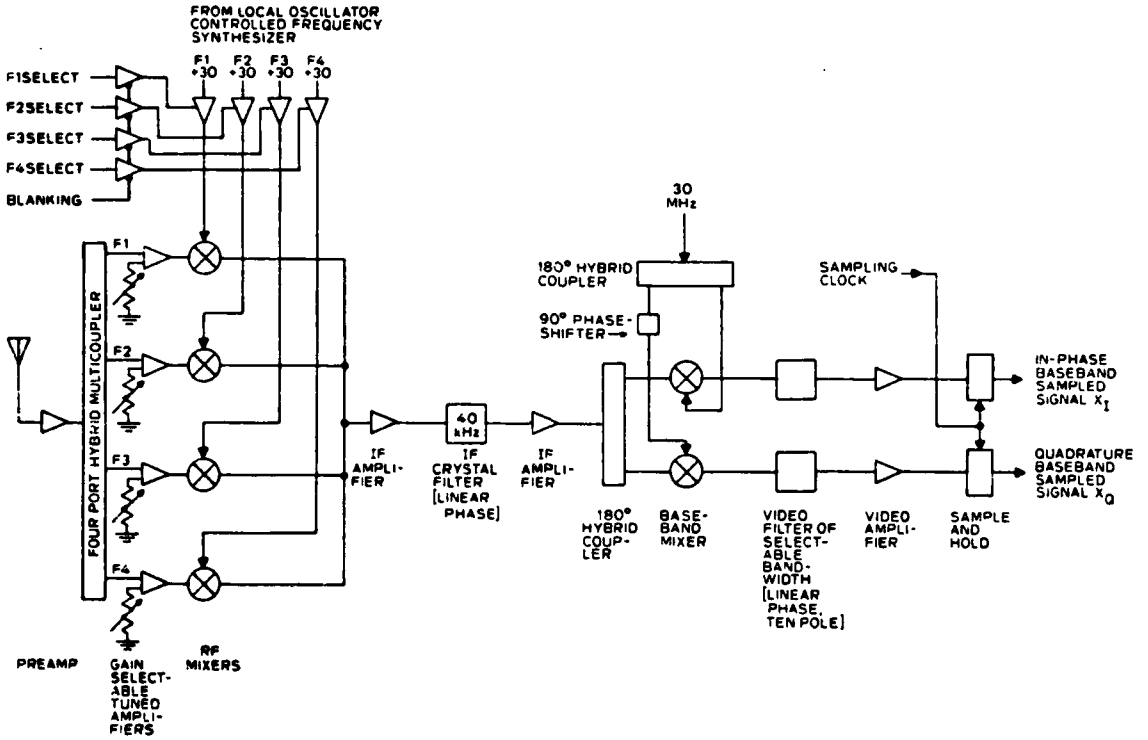

a. Dual-conversion superheterodyne analog system

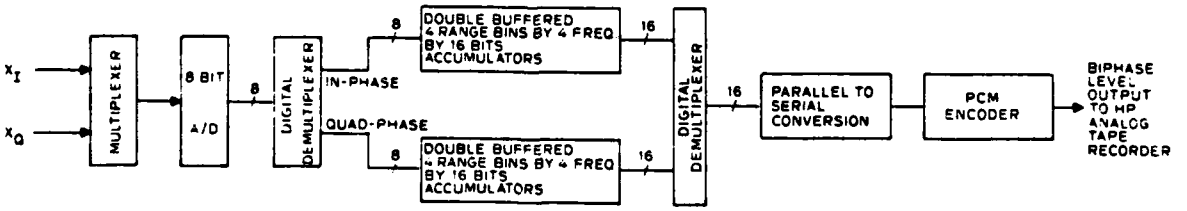

b. Digital system

Figure 1

Receiver system for the Stanford four-frequency radar.

bandwidth. The signals are then amplified to a 50 W peak power level by a commercial wideband amplifier to form the final transmitter output. All of the phase-locked loops are referenced to a stable 3 MHz crystal oscillator. The use of the double loops means that the original 8:1 frequency range can be covered by oscillators which need cover

only a 2:1 frequency range.

3.2 Receiver

A block diagram of the receiver portion of the radar system is shown in Figure 1a. The receiver consists of four separate amplifiers, each fixed-tuned to one of the transmitter frequencies and followed by a balanced mixer driven by one of the same 34–60 MHz loops used to drive the transmitter (but gated on for a full 400 μs). The outputs of all four mixers are common. This generates a first intermediate frequency (IF) of 30 MHz. After amplification at 30 MHz, the signal is mixed with the same 30 MHz transmitter translation loop in a second mixer to produced a second IF centered at 0 Hz. The use of in-phase and quadrature local oscillator signals at the second mixer allows the separation of positive and negative Doppler shifts, so that approaching waves can be distinguished from receding waves.

3.3 Data sampling and recording

After suitable amplification at the second IF, the echoes are sampled with 8-bit resolution at four different time delays (corresponding to four different radar range cells) after the transmit pulse. Both the time delay from the transmit pulse and the spacing between samples can be selected in 10 μs steps. In normal operation, the samples are taken at intervals of 40 μs, starting 50 μs after the transmitted pulse, which gives a range resolution of 6 km. A number of such complex samples are added together in a 16-bit accumulator, both to improve the signal-to-noise ratio and to allow the use of a low peak power transmitter by using a high pulse repetition rate. The number of such pulses added together can be varied, but it was usually set so that the effective sampling rate was approximately 2 Hz. This allows Doppler frequencies in the range of -1 Hz to $+1$ Hz to be resolved.

The digital processor is shown in Figure 1b. The samples are accumulated in 16 separate accumulators, one for each range cell at each frequency. Each one is 32 bits

wide: 16 bits for the real part and 16 bits for the imaginary part. There are two complete sets of buffers, so that one set can be filled while the other set is being recorded. The resulting 16-bit sums, along with all the radar system paramaters, are recorded in digital form as a pulse-code modulation (PCM) waveform on a 1/4 inch analog instrumention tape recorder. For the shipborne experiment, the receiving antenna was composed of 8 elements and each one was sampled separately, so a total of 128 separate complex time series were recorded.

Chapter 4

The Pescadero Experiments

The Pescadero experiments were designed to study the effects of vertical current distribution, determined by *in-situ* measurements, on the radar signals. Consequently, a one-dimensional geometry was adequate, and the antenna system provided a narrow beam for all four frequencies fixed in one direction. On the other hand, the JASIN measurements were an application of the technique to obtain oceanographic data in the open ocean, and some degree of antenna steering capability was required. As a result, the antenna systems were quite different for the two experiments.

4.1 Radar installation

On several occasions between May 1975 and January 1978, HF radar backscatter observations of the ocean surface were made from a site on the California coast near Pescadero. A map of the site of the experiment is shown in Figure 2. The site was located about 1 km from the coast, as indicated in Figure 3. For these experiments, the radar was operated on frequencies of 6.78, 13.38, 21.77 and 29.80 MHz. These frequencies are in Bragg resonance with ocean waves of length 22.1, 11.2, 6.9 and 5.0 m.

The transmitting antenna was a vertical half-rhombic antenna, approximately 250 m long and 45 m high at the apex, supported by a large helium-filled balloon. This antenna system was chosen to provide a moderately directional, wideband transmitting antenna at a reasonable cost. It required no fixed towers to install and maintain. It

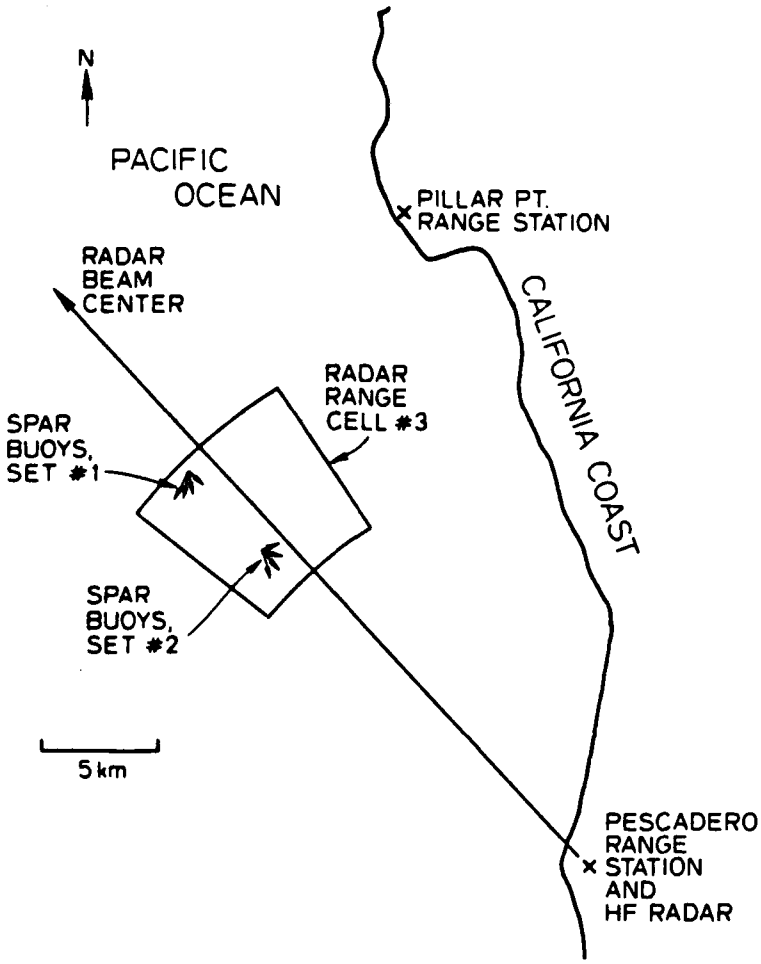

Figure 2
Site of the Pescadero experiment, showing the locations of the spar buoys and range stations.

did have the disadvantage that the balloon had to be filled with helium before each experiment, so it required about an hour to set up the antenna. Operation of the antenna was limited to wind speeds of about 15 $m\,s^{-1}$ at the radar.

The receiving antenna was a single wide-band air-core loop one metre in diameter, manufactured by Hermes Company. The loop had a matched preamplifier installed right at the loop. The combination of the loop antenna and matched preamplifier resulted in an antenna which had an effective height of one metre over the entire 3–30

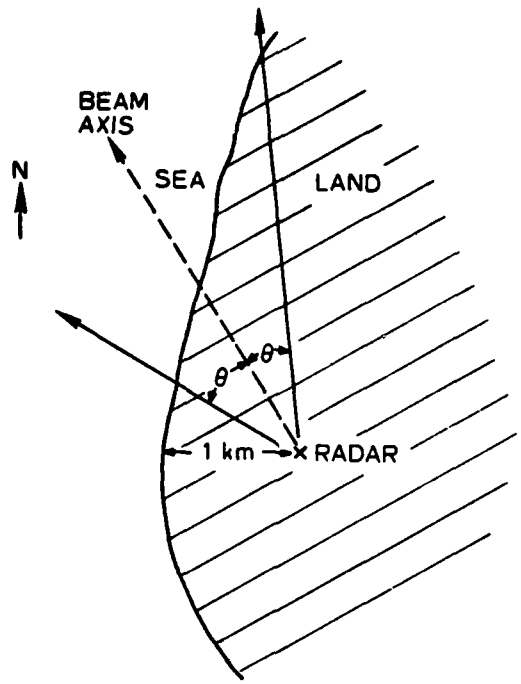

Figure 3
Propagation paths over land. This is a rough sketch of the coastline; small-scale details are ignored.

MHz frequency range. Because of the fixed transmitting antenna, the system antenna pattern was fixed about a nominal center direction of 315° T. The 3 dB full width of the composite radar beam varied between 50° and 12°, as shown in Figure 4. The measured beam center direction varied from 320°T at 30 MHz to 290°T at 4 MHz as a result of the propagation path over land.

Observations were usually made four times each month and typically consisted of four half-hour runs, each with a different radar pulse width. Wind speed was recorded locally and at several coastal sites operated by the National Weather Service. Several observations which included both the Scripps pitch-roll buoy [*Stewart*, 1977] and *in-situ* drifter measurements of the ocean current were made from 10–27 January 1978; these observations are included in this report. The locations of the spar buoys and the radar range cell footprint are shown in Figure 2. For these observations, the wind speed was

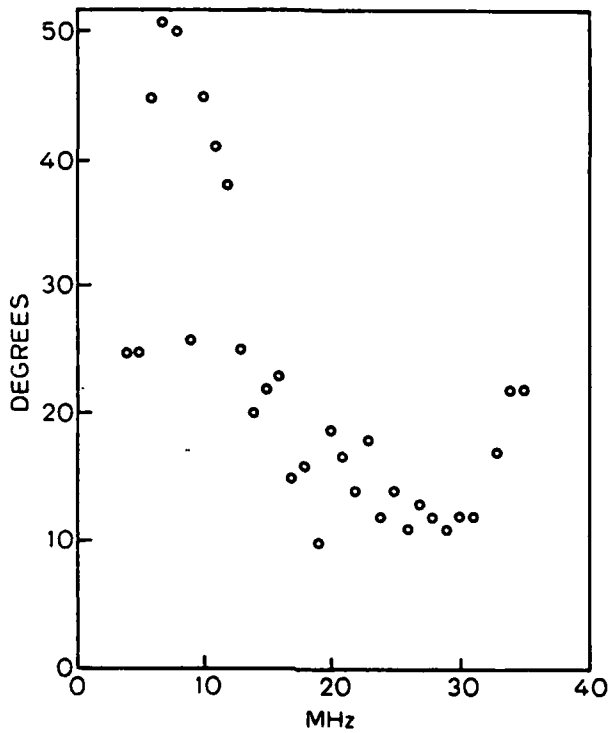

Figure 4
Measured 3 dB full width of the composite Pescadero antenna *vs.* radar operating frequencies.

also recorded on the boat used to deploy the buoys.

4.2 Spar buoys

The drifters were four lengths of spar buoys made of plastic pipes loaded with sufficient lead shot so that they immersed upright in water to predetermined depths of 1, 3, 6, and 12 m. The locations of the buoys were determined by a microwave tracking system which had a range resolution of a few metres. The boat used to deploy the buoys carried the master station which continuously interrogated two transponders located about 30 km apart on the coast. The position of each buoy was measured by carefully maneuvering the boat to within a few meters of the buoy and then noting the range to each of the two transponders. The position measurements were repeated at time intervals of an hour or longer, and velocities were calculated from the differences in

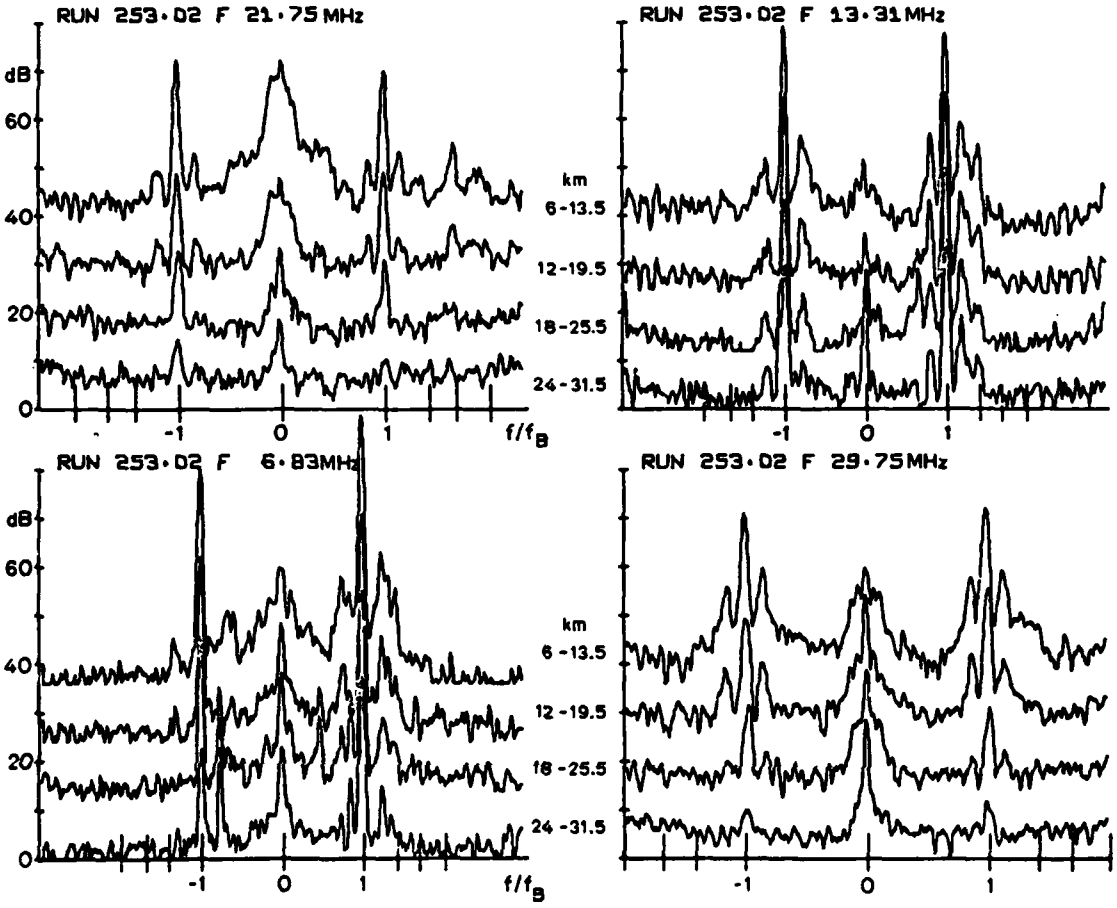

Figure 5
Smoothed Doppler spectra at four radar frequencies and four range cells. Data were collected at Pescadero on 25 January 1978.

position. Because the buoys typically drifted on the order of 1 km, the uncertainty of the drift velocity was less 1% [*Ha*, 1979].

The buoys were not completely immersed in the water; for visibility, a portion of the buoy, 10–25% of the buoy length, was exposed to wind drag above the water surface. Ha calculates that the effect of the wind drag on the buoy velocity is less than the statistical uncertainty in the buoy-inferred drift. He also demonstrates that a buoy immersed to depth d will drift with a speed equal to the current at a depth of $0.5d$ and $0.27d$ for a current varying linearly and logarithmically with depth, respectively.

To obtain an indication of the variation of ocean current within a single radar range

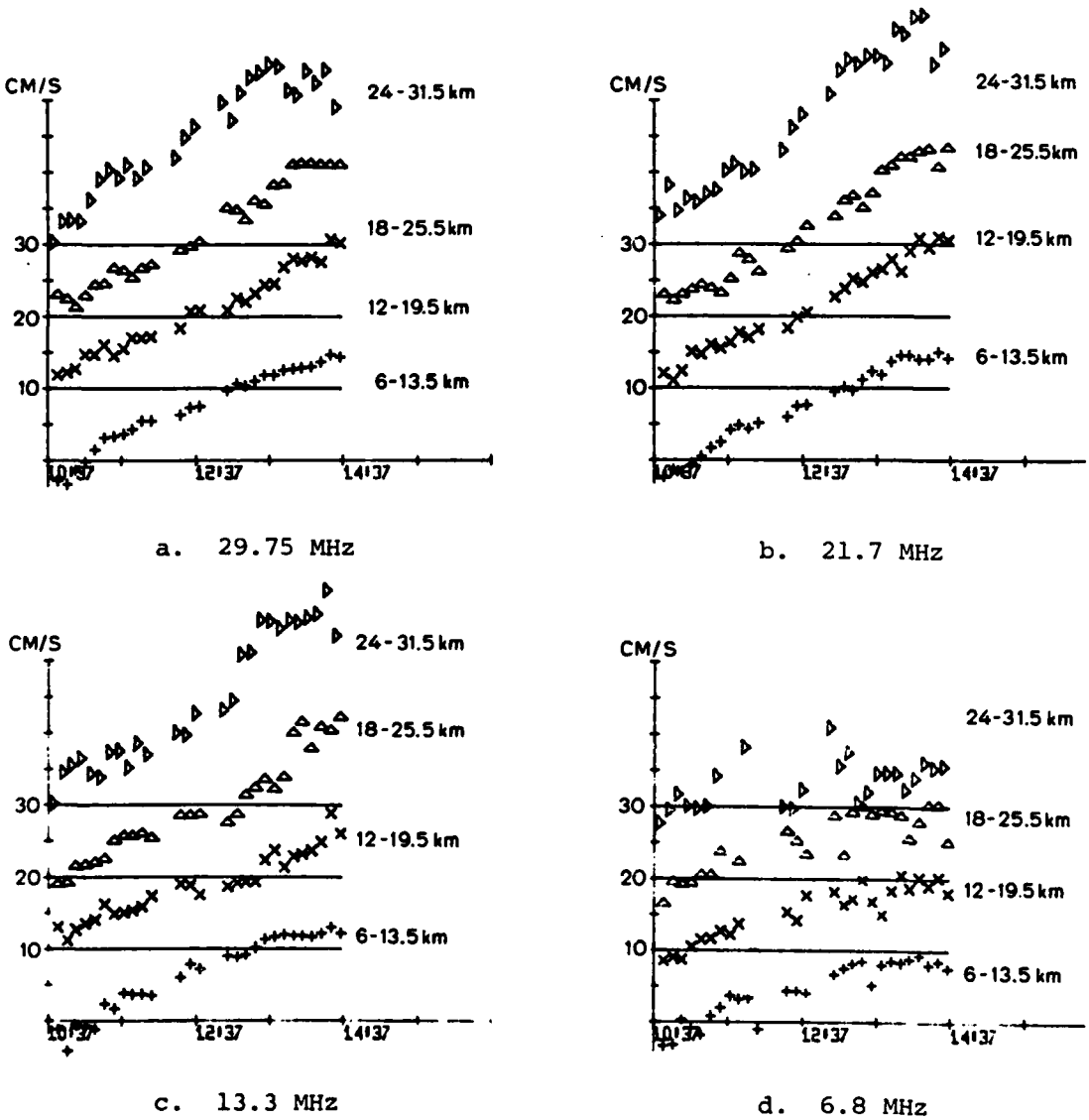

Figure 6

Radar-inferred depth-averaged current at four range cells *vs.* time during 25 January 1978. Horizontal lines are the baselines for the different range cells.

cell, two sets of buoys separated by approximately 5 km were deployed within the third range cell of the radar system. Because only one boat was used, the measurements of current at these two points were also separated by 30–60 minutes, the time required by the boat to move from one location to the next and to find the buoys.

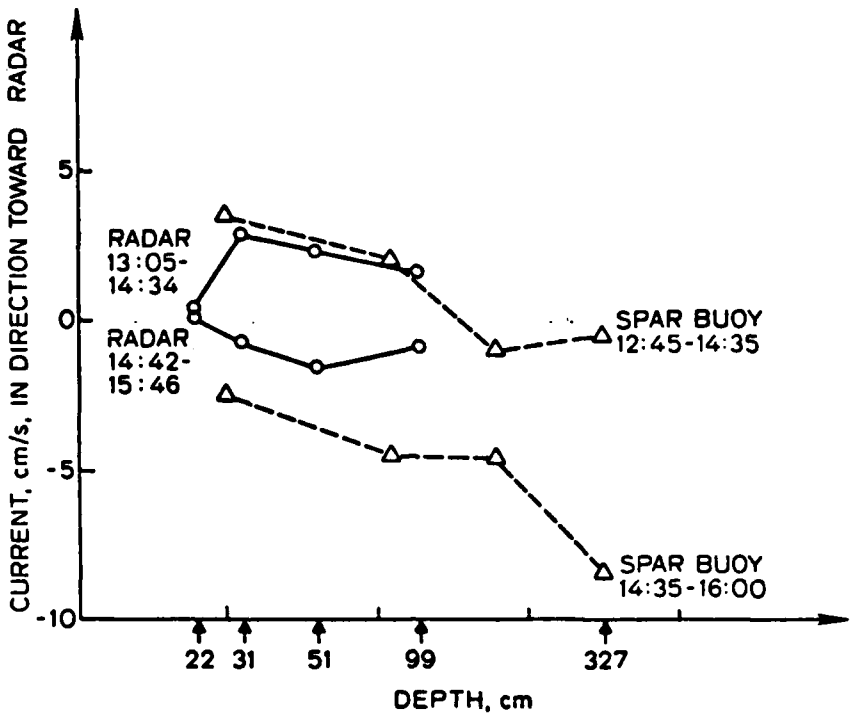

Figure 7
Comparison of radar-inferred drift and spar-buoy drift (cluster 2) obtained on 19 January 1978. The horizontal axis is logarithmic in depth, and a logarithmic profile is assumed. The approaching Bragg line was used.

4.3 Data processing

The radar echoes at four different frequencies were each sampled at four range cells approximately twice a second for a total period of 2–4 hours for each data run. Fourier transforms were computed for each 10-minute data segment. The first-order echoes were extracted by first searching for the peak of the power spectrum in a narrow region centered on the theoretical position of the Bragg line. Then the null between the first-order peak and the second-order continuum on either side of the Bragg line was found by searching for the points at which the local slope of the smoothed frequency spectrum changed sign. The nulls thus found defined the limits of the first-order energy band. The centroid of the first-order spectrum (the first-order moment) was found by integrating the spectrum over this range. The frequency corresponding to the centroid

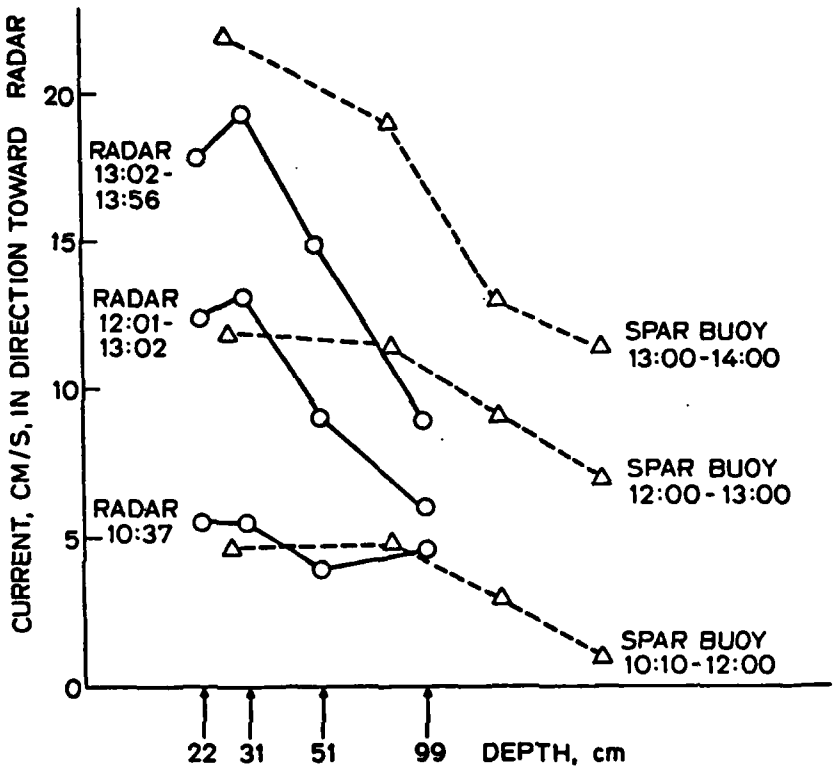

Figure 8
Comparison of radar-inferred drift and spar-buoy drift (cluster 1) obtained on 25 January 1978. The horizontal axis is logarithmic in depth, and a logarithmic profile is assumed.

of the spectrum was taken as the measured frequency of the Bragg line. The theoretical Bragg frequency was subtracted from the measured frequency, and this difference was converted to a current velocity by $v = f\lambda/2$. Details of the data processing are described by *Ha* [1978] in his Ph.D. thesis. The use of this centroid calculation was quite effective because the antenna beam width was relatively narrow, as noted above.

An example of the smoothed radar frequency spectra at the four radar frequencies and four range cells is shown in Figure 5. The first-order Bragg lines at $\pm f_B$ are used to determine the current. Note that the nulls between the first-order lines and the *second-order continuum are well-defined. They usually could be found reliably by the* algorithm described above. The altorighm was not sensitive to the land echoes centered

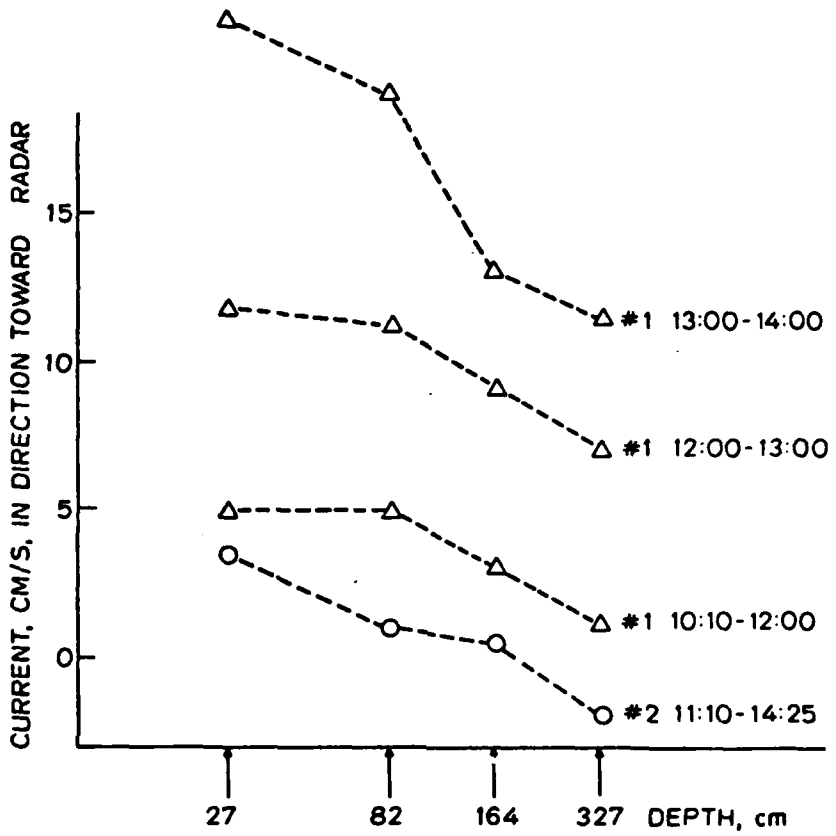

Figure 9
Variance in drifts of spar buoys released in the same range cell. Cluster 1 was released at 25.8 km from Pescadero, and cluster 2 was released at 20.5 km. Data were collected on 25 January 1978.

at DC, or to signals beyond a narrow region centered on the Bragg line.

4.4 Results

Radar-inferred currents are shown in Figure 6. There is a strong time-dependent tidal component, but in addition, there is variation both in range and with radar frequency. Figures 7 and 8 show the comparison between the radar-inferred current and the spar-buoy drift on 19 January and 25 January 1978, respectively. For these figures, it was assumed that the current varies logarithmically with depth, an assumption which appears to be justified by numerical inversion of some of the radar data [*Ha*, 1978].

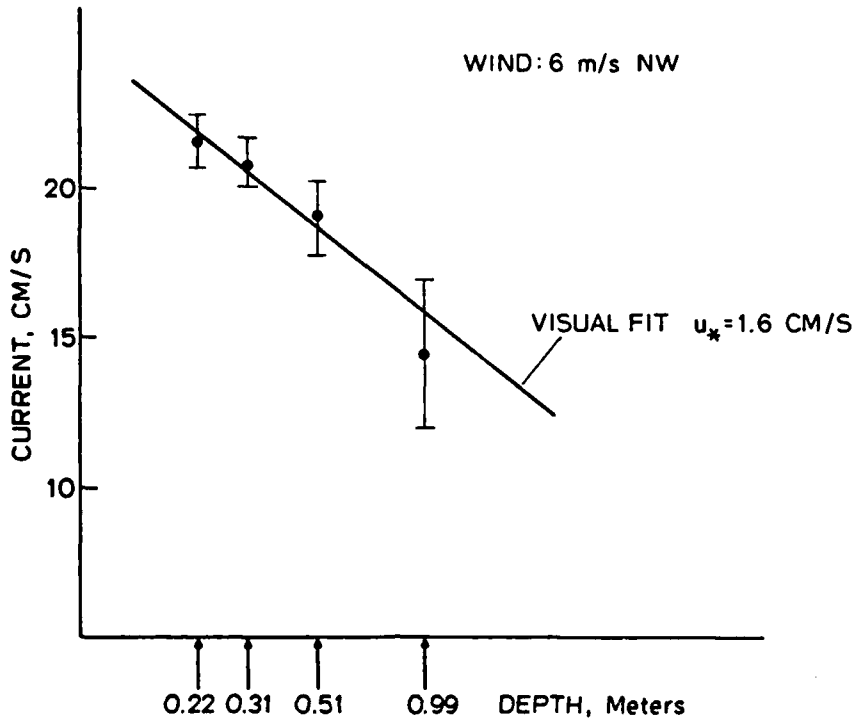

Figure 10
Logarithmic current shear measured by the four-frequency radar. The horizontal axis is logarithmic in depth, and a logarithmic profile is assumed in the inversion. Vertical bars indicate the resolution limited by a finite-time Fourier transform. Data were obtained at Pescadero at approximately 14:15 to 15:15 local time; range 6 to 13.5 km.

The radar and the buoy measurements show similar changes of current with time which are apparently related to the tidal cycle. Also, the radar and buoy measurements show similar decreases of current with depth. On 25 January, both the radar and buoy data show a vertical gradient in the measured current which increases with time. This can be explained in part by a rise in the wind speed in the direction toward the radar. However, the magnitude of the vertical shear as measured by the radar is 4–6 times the value predicted by (8) from the wind speed, and the shear measured by the buoys is also higher than would be predicted from the waves alone.

Figure 9 illustrates the variance in the drifts of spar buoys released in the same

Summary of Measured and Predicted Shears – Pescadero				
Date, 1978	Radar meas.	Total est.	Wind est.	Wave est.
19 Jan	0.91	4.81	1.78	3.03
24 Jan	4.69	2.73	1.55	1.18
24 Jan	9.50	2.73	1.55	1.18
25 Jan	1.07	1.74	1.40	0.34
25 Jan	7.08	1.74	1.40	0.34
25 Jan	9.80	1.74	1.40	0.34
27 Jan	9.95	4.95	3.18	1.77
27 Jan	13.31	4.95	3.18	1.77

Table 1

Summary of Pescadero radar measurements and wind- and wave-predicted values for the current shear. The radar values represent the difference in $\mathrm{cm\,s^{-1}}$ between the current velocities obtained from radar measurements of 5.0 m and 22.1 m ocean wave phase velocities. The wind and wave estimates of the shear are based on the difference in current velocities predicted for depths of 21 cm and 93 cm, respectively. These are the depths at which the 5.0 m and 22.1 m waves are coupled to the currents, assuming a logarithmic current profile.

range cell. It is evident that the two sets of buoys, separated by 5 km, give quite different results. In fact, by comparing Figures 8 and 9, it appears that there is better agreement between the radar measurements and either set of buoy measurements than between the two sets of buoy measurements. This is an indication of the horizontal variability of the current field. Because the radar illuminates a finite-sized range cell approximately 7.5 km deep, the radar measurement represents an average rather than a point measurement, so the two methods cannot be directly compared.

Figure 10 illustrates the current shear measured by the radar on 24 January, and shows that a logarithmic variation of current with depth provides a good fit to the data. The slope of a visual fit to the data points provides an estimate of 1.6 $\mathrm{cm\,s^{-1}}$ for u_*, a value about twice what would be predicted from the wind speed of 6 $\mathrm{m\,s^{-1}}$.

Table 1 summarizes the vertical current shears measured by the HF radar system in several experiments during January 1978. Also listed are values of vertical current shear which would be predicted by (8) and (3) from the wind and wave conditions present at the times of the experiment. The radar measurements showed a wide variability, but in

general they were several times higher than would be predicted by the wind or waves alone, or the sum of the two predictions, assuming colinear directions. The Pescadero results shown in Table 1 are also included in the plots in Chapter 5.

Chapter 5

The JASIN Experiment

During the summer of 1978, the Joint Air-Sea Interaction (JASIN) experiment was conducted in the North Atlantic Ocean off the coast of Scotland. The overall goal of this international experiment was to measure the momentum transfer between the wind and the waves. Most of the oceanographic measurements were conventional, depending on tethered buoys supporting current meters, thermistors, and anemometers; pitch-roll buoys for measuring wave height and direction; and instruments lowered from ships for measuring the temperature, salinity and density of the deep ocean water. In addition, daily observations of HF radar backscatter were made throughout the experiment to determine if a vertical current shear could be measured from a platform in the open ocean.

5.1 Radar installation

The four-frequency radar was installed on the R. V. *Atlantis-II* and measured velocities relative to that platform; ship drift can be estimated from the shipboard Loran-C navigation system. The ocean-wave directional spectrum was measured simultaneously with the radar observations by a pitch-roll buoy. The directional spectrum of the ocean waves can also be inferred from the directional distribution of the echo energy arriving at the radar.

The transmiting antenna consisted of a set of quarter-wave vertical radiators and was nominally omnidirectional. Figures 11 and 12 show the transmitting antenna.

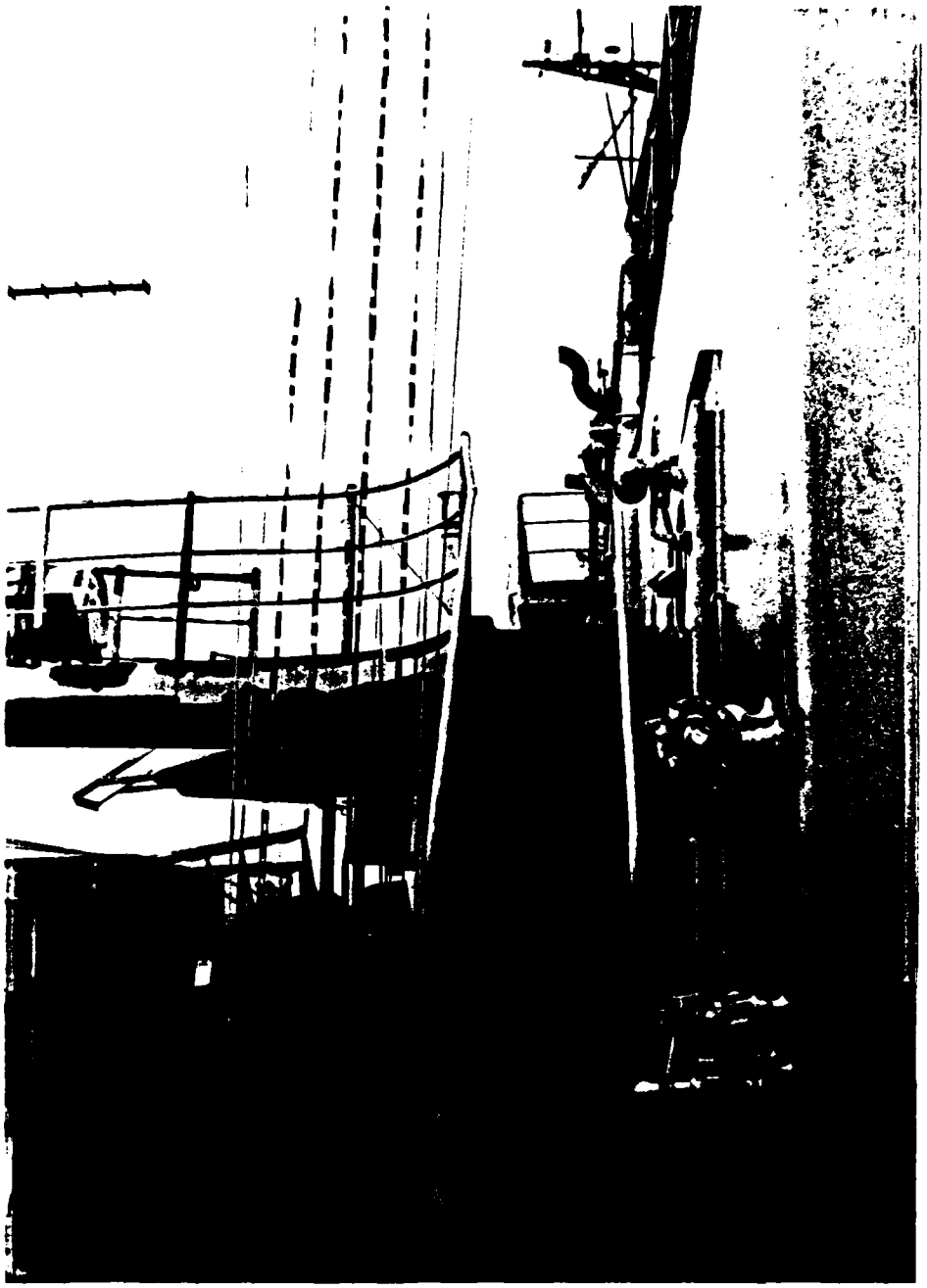

Figure 11

View of the base of the JASIN transmit antennas. There were four quarter-wavelength antennas, all fed in parallel from a common cable. The ship was used as the ground plane. The elements themselves were made of two-conductor transmission line (with both leads tied together) to lower the Q of the antenna so that the 50 μsec pulse could be passed without severe distortion caused by a narrow-bandwidth antenna.

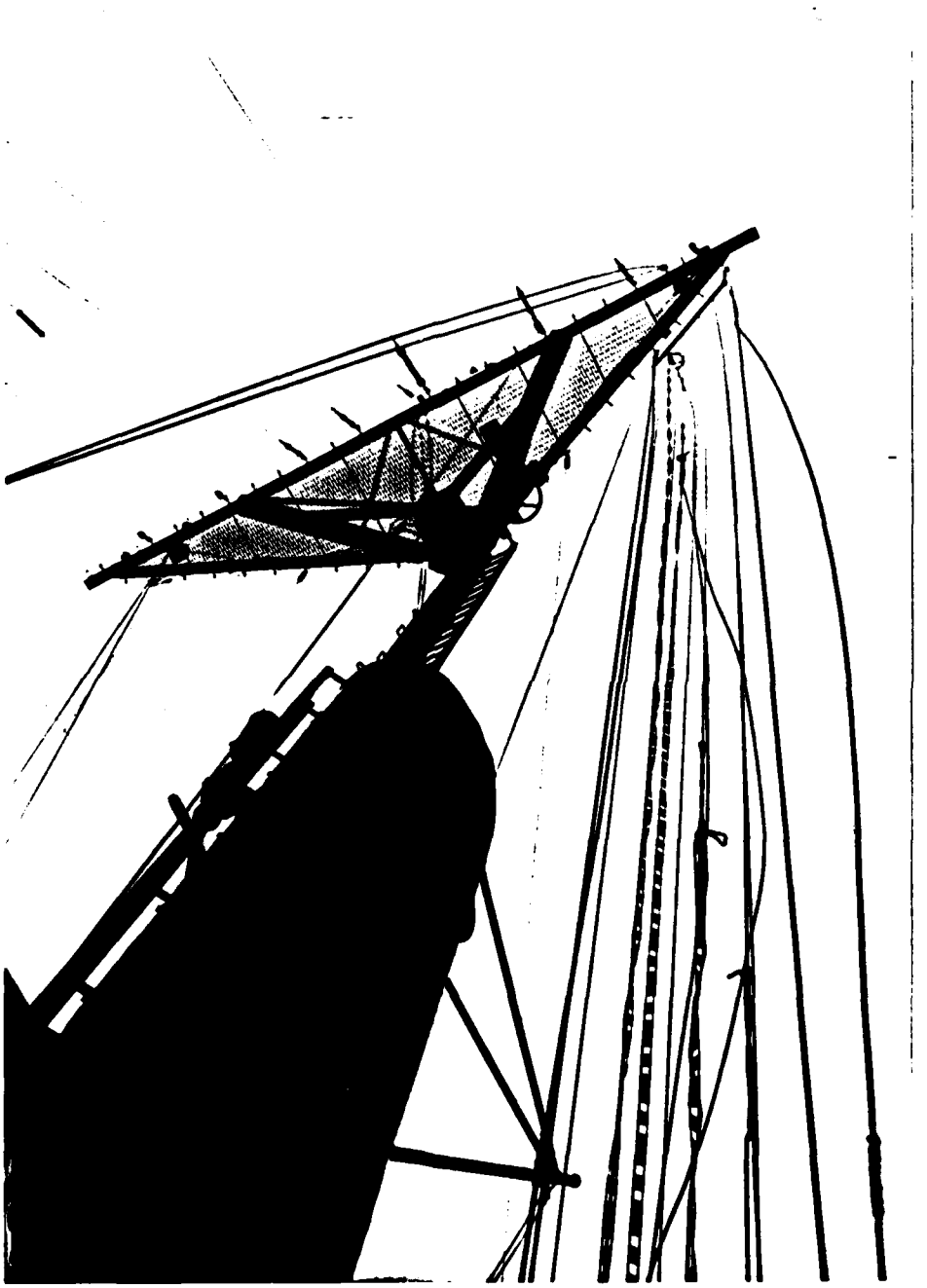

Figure 12
View of the top of the JASIN transmit antennas. The elements were suspended from the mast and kept taut by individual ropes.

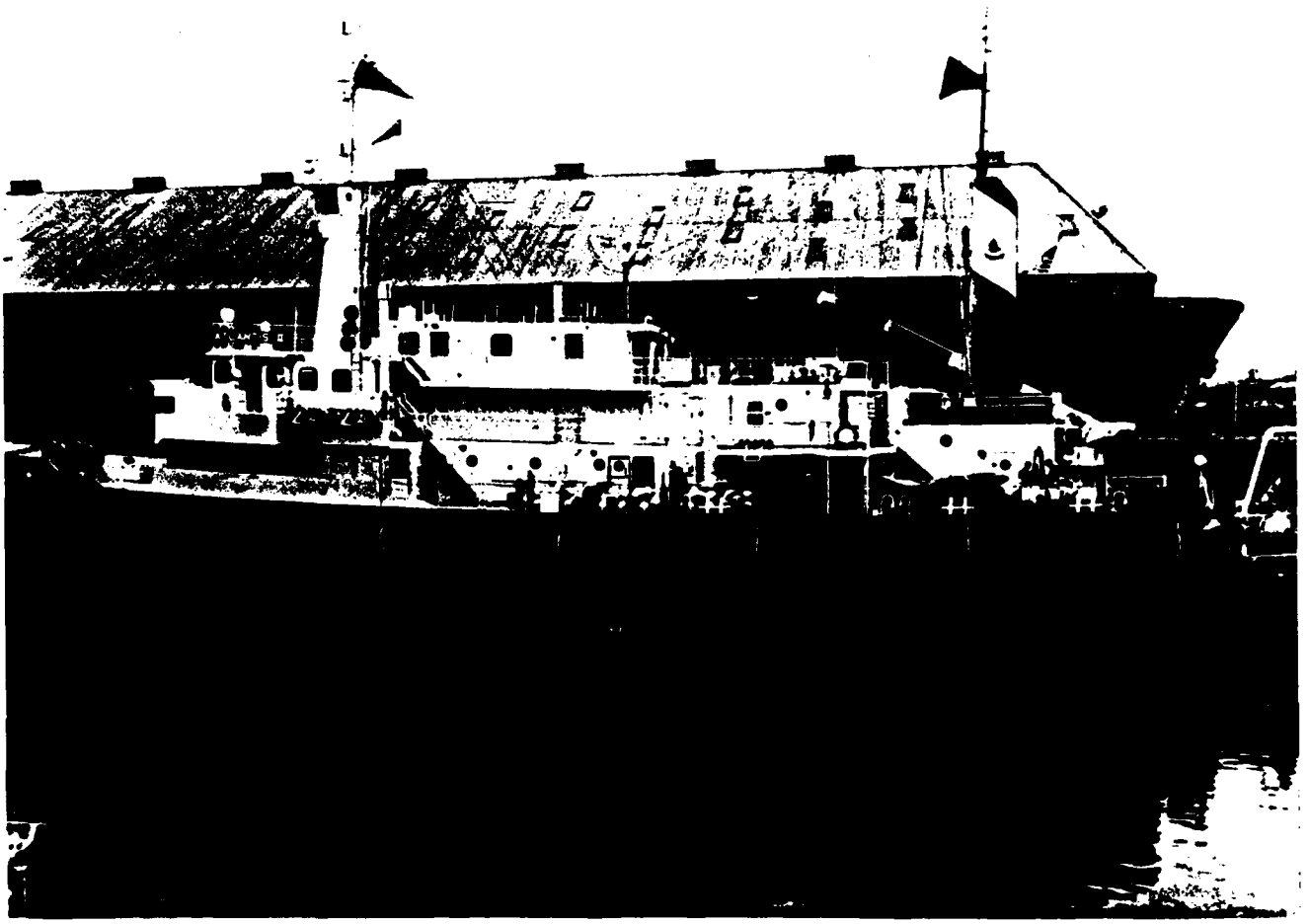

Figure 13
View of port side of *Atlantis-II* at the dock in Glasgow. The receiving array is visible along the side of the ship as six light-colored loop antennas (seen edge-on), each with an associated preamplifier immediately above the antenna element. The transmitting antenna was not installed at this time.

System directivity was provided by an array of eight broadband loop receiving antennas, six on the port side of the ship and two on the starboard side. The six antennas on the port side are shown in Figure 13, and the individual elements are shown in more detail in Figure 14. The loop elements, approximately 1 m high, were constructed as half-loops and made use of the ship hull to provide an image half-loop. A wideband preamplifier was mounted immediately above each loop.

The loops were selected, one at a time, by an electronic switch preceding the radar receiver. Thus, the signals from the individual loop elements were recorded separately.

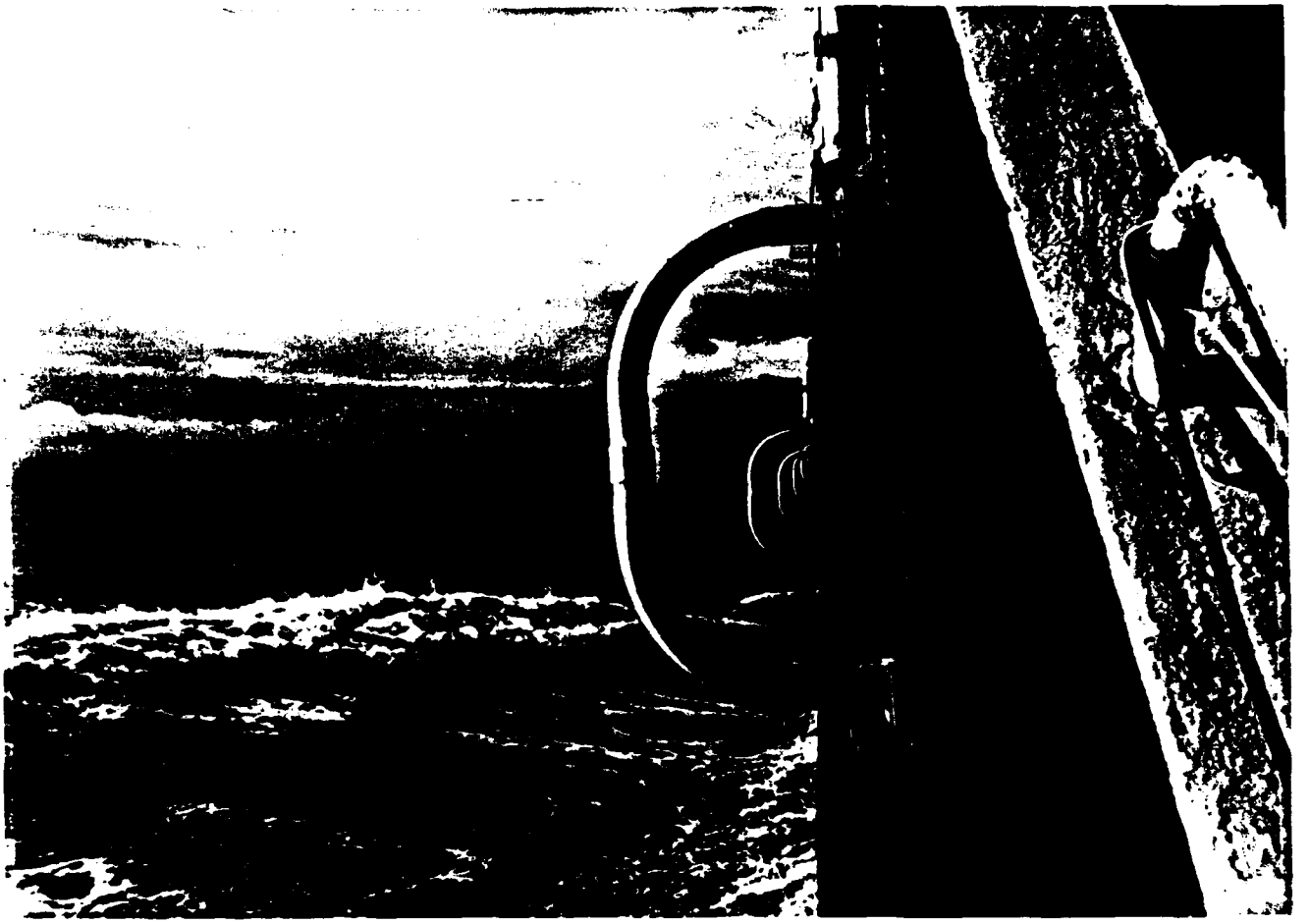

Figure 14
View along the axis of the receiving array, showing several of the individual elements and preamplifiers. The loops and preamplifiers were broadband, covering the 3–30 MHz range without tuning. The elements were designed so that they could easily be removed from their mounting brackets when the ship docked.

By varying the relative complex weights applied to the signals from each receiving element, the radar beam can be steered in several directions, so that the velocity measurement can be made in several directions.

The beam formation was done in software in the frequency domain. The total array aperture was approximately 40 m, and the half-power beamwidth was between 45° and 15°, depending on the frequency and direction of steering the array. The azimuthal response of each of the loop elements (in combination with the transmit antenna) was

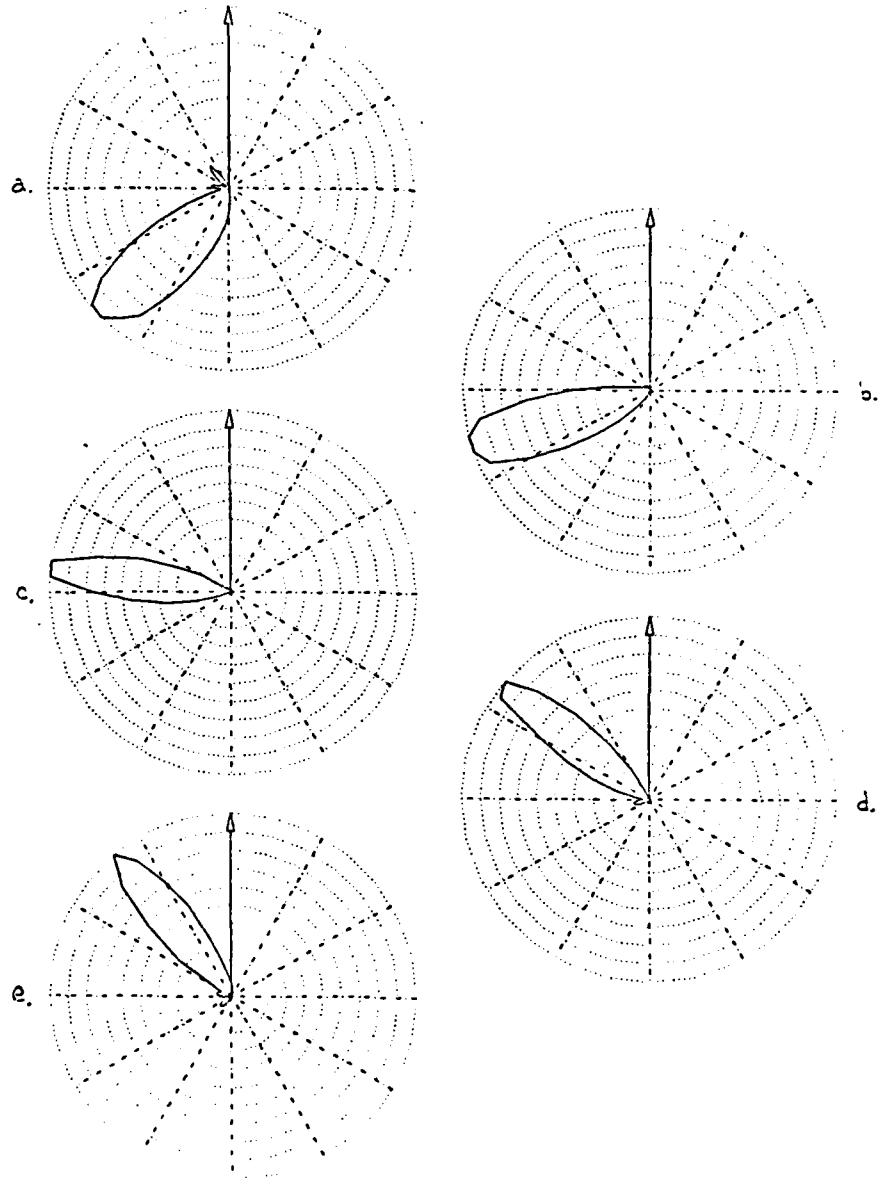

Figure 15

Plots of the combined transmit-receive pattern at 13.38 MHz. The plots are linear in power. The direction of the bow of the ship is indicated by the arrows. The beam has been steered in all 5 directions from the same data set by multiplying the signals from the individual elements by appropriate complex weights. The patterns were measured by using a transponder on the *Meteor* while the *Atlantis-II* was slowly turned in a circle.

measured by using a transponder on another ship, the R. V. *Meteor*, and by using these data the combined array pattern could be computed. The shape of the array pattern changed as the beam was steered; it was not a fixed pattern which was simply rotated in space. Figure 15 shows the antenna power patterns which were achieved at 13 MHz.

The radar was operated on frequencies of 4.80, 6.78, 13.38, and 21.77 MHz, which are in Bragg resonance with ocean waves of length 31.2, 22.1, 11.2, and 6.9 m. Coherent processing of the radar signals for a period of approximately 10 minutes provides a frequency resolution of 1.6 mHz, from which the Doppler shift of the radar target can be measured with a resolution of 4.8 $\mathrm{cm\,s^{-1}}$ for the longest wavelength and 1.2 $\mathrm{cm\,s^{-1}}$ for the shortest.

5.2 Data processing

The majority of the data procesing was concerned with estimating the current shear. However, in a related study, *Elabdalla* [1982] examined the use of super-resolution spectral estimation techniques to estimate the ocean-wave directional spectrum.

5.2.1 Estimating the current

To first order, the radar responds only to those ocean waves which have a wavelength L equal to one-half the radar wavelength λ, and which are traveling radially toward or away from the radar. The phase velocity v_P of these Bragg-resonant ocean waves imparts a Doppler shift of $f_B = 2v_P/\lambda$ to the radar signals, where $v_P = \sqrt{gL/2\pi}$, g is the gravitational acceleration and $L = \lambda/2$. This Doppler shift is independent of the direction of arrival of the ocean echoes, because the radar is only sensitive to those waves which are travelling exactally radially to the radar. In addition, if there is a current present with a component v_C in the direction of the radar beam, then if the radar beam is sufficiently narrow there is an additional Doppler Shift of $2v_C/\lambda$ due to this current component. For a land-based narrow-beam radar, the current can be estimated directly from the measured Doppler shift of the radar echo.

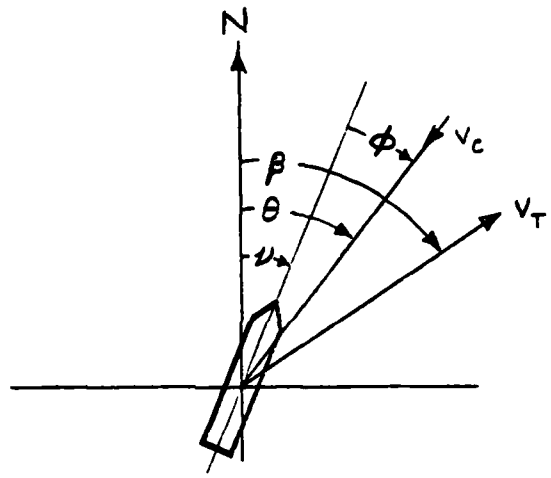

Figure 16
Geometry for a radar on a moving platform. The ship heading is ν and the ship is drifting in a direction β with a velocity v_T. The radar is receiving echoes from a target with a velocity v_C from a direction θ. The antenna pattern is fixed relative to the ship, and the echoes are seen by the antenna at a relative direction ϕ.

However, the situation is more complicated if the radar is mounted on a moving platform, such as a ship, and if the antenna pattern is broad, as it was during the JASIN experiment. A typical geometry is shown in Figure 16. If the ship is moving in a direction β with a velocity v_T with respect to the water, there is an additional Doppler shift of $(2v_T/\lambda)\cos(\theta-\beta)$, where θ is the direction from which the radar signal arrives. (The absolute current and the ship drift can be lumped together; it is only the *relative* motion which is measured.) In the absence of any relative motion between the ship and the water, the frequency spectrum of the first-order Bragg echo appears as two very sharp lines at $\pm f_B$; the ship drift spreads these into two bands of frequencies (much as a synthetic aperture radar does) which extend $\pm 2v_T/\lambda$ from the Bragg center.

The shape of the frequency spectrum between these limits depends on the directional distribution of ocean energy, the shape of the radar antenna patterns, and the Jacobian of the transformation between angle-of-arrival and frequency. For a given frequency $f < f_{max}$ where $f_{max} = 2v_T/\lambda$, the angle of arrival relative to the ship is

$\pm\cos^{-1}(f/f_{max})$; the $\pm$ arises because $\cos(\theta)$ is an even function of θ. Defining

$$\begin{aligned}
S(\theta) &= \text{ocean-wave directional spectrum:} \\
&\qquad \text{energy density / unit angle for waves arriving from } \theta \\
a(\phi) &= \text{antenna power pattern in direction } \phi \text{ from the bow of the ship} \\
\nu &= \text{heading of the ship} \\
v_T &= \text{magnitude of ship drift relative to water} \\
\beta &= \text{direction of ship drift relative to true north} \\
f_{max} &= 2v_T/\lambda,
\end{aligned} \tag{10}$$

then one would expect the frequency spectrum of the radar signal to be given by

$$E_j(f) = \sum_{i=1}^{2} S(\theta_i(f))a_j(\theta_i(f)-\nu)\frac{1/f_{max}}{\sqrt{1-(f/f_{max})^2}}$$

where

$$\theta_i(f) = (-1)^{i-1}\cos^{-1}(f/f_{max}) + \beta. \tag{11}$$

with the beam steered in the jth direction.

In order to estimate the current shear, it is necessary to solve equations (10) and (11) for v_T and β at the four different radar wavelengths. In order to do this, a curve-fitting procedure was used, based on a model the ocean-wave directional spectrum as a single-peaked distribution of the form $\cos^s((\theta-\theta_0)/2)$. The values for the ocean model parameters s and θ_0 could be obtained from the Scripps pitch-roll buoy measurements, from synthetic aperture HF radar data taken during the experiment, or left as free parameters. Typically, the directional distributions during JASIN had a half-power beamwidth of 30° or less, much narrower than were found by *Tyler et al.* [1974] at Wake Island. In this case, the effective direction in which a current measurement is made depends more on the ocean directional distribution than on the antenna pattern.

The antenna beam was formed in five different directions covering a 90° range, and the frequency spectrum of the radar echo was computed for each of these directions. The frequency estimate $E(f)$ was computed for each of these directions and was compared with the measured spectrum (the shape of $a_j(\phi)$ is different for each beam direction

j). An error measure over all five directions was computed, and this was minimized by varying the parameters v_T and β (and in some cases s and θ_0 as well) until a minimum overall error was achieved.

Early attempts to measure the vertical current shear using a land-based radar estimated the position of the shifted Bragg line by noting the peak of the frequency spectrum [*Stewart and Joy*] or by calculating its centroid [*Ha*]. Such procedures inherently assume that the radar antenna beamwidth is sufficiently narrow that the antenna selects only echoes (and hence current components) along a very narrow direction. Although this assumption was valid for the Pescadero experiments, it was not valid for the JASIN experiment, and echoes from as much as 90° can contribute to the observed frequency spectrum. In this case, the detailed shape of the frequency spectrum (and hence its centroid) is highly dependent on the shape of the ocean directional spectrum and the antenna pattern. The curve-fitting procedure described above was originally implemented with a gradient search over the parameters of the models for both the ocean directional spectrum and the current, but the data were too noisy for this approach to be stable. Consequently, the model parameters for the ocean directional spectrum were fixed at those estimated from the buoy measurements, and the current magnitude and direction were left as free parameters to be found by a straightforward sequential search. Finally, the search was repeated on just the magnitude of the current, with its direction fixed at the average value determined in the last step. This procedure was applied to the data from each of the four range bins at each of the four radar frequencies.

Once the apparent current was obtained for each radar wavelength, a linear regression analysis was applied to the radar-inferred current as a function of the logarithm of the ocean wavlength. The shear was taken as the difference in currents given by the intercepts of this line at the the minimum and maximum depths probed by the radar. The shear value was retained only if the correlation coefficient of this fit was greater than 0.20, and only if at least 3 of the 4 radar frequencies were used (in some cases, individual frequencies were omitted because of strong interference identified by

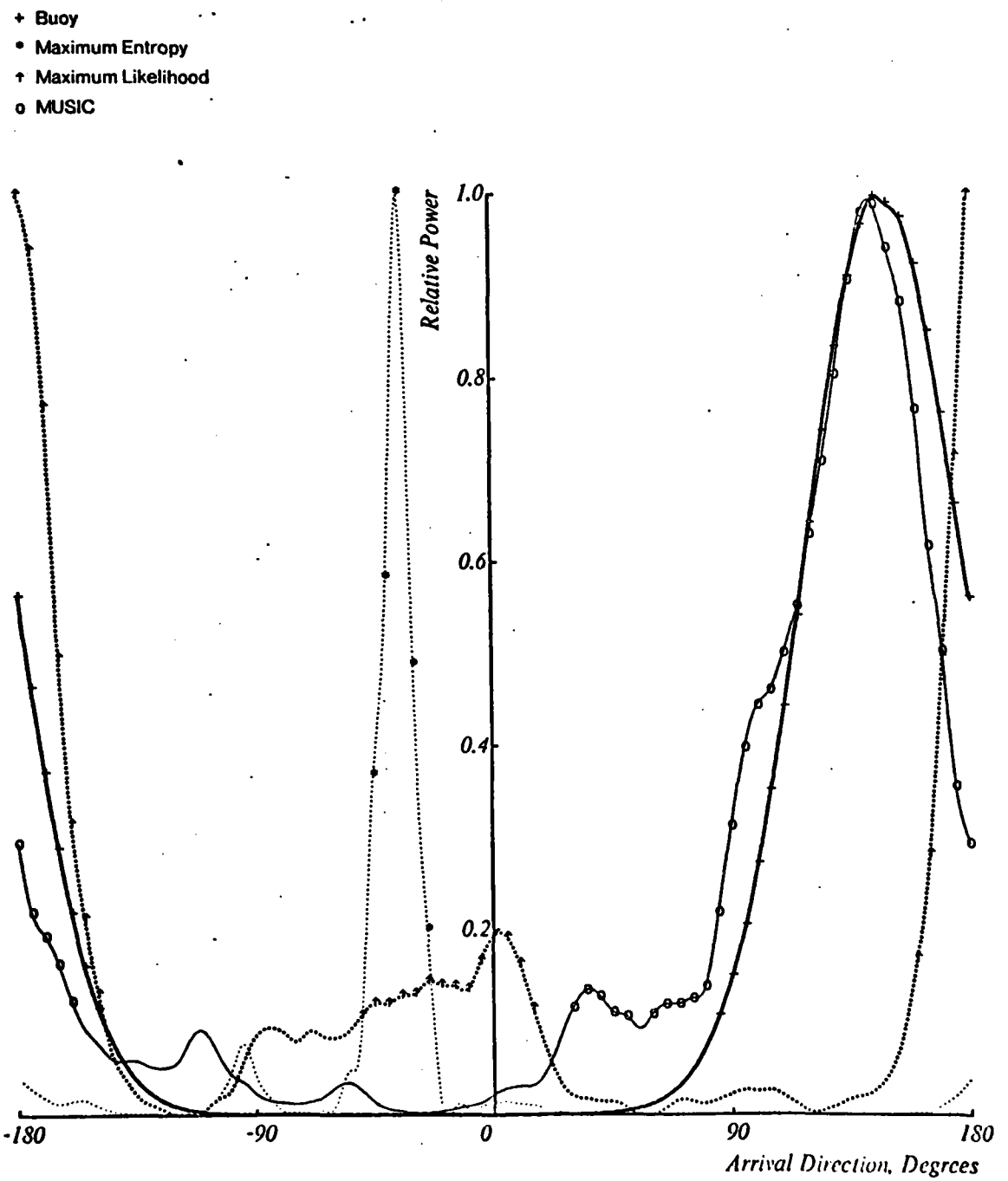

Figure 17
Buoy, ME, ML, and MUSIC spectrum estimators. 5 Sept. 78, 4.80 MHz. The vertical scale is linear in relative power. The x-axis represents degrees True.

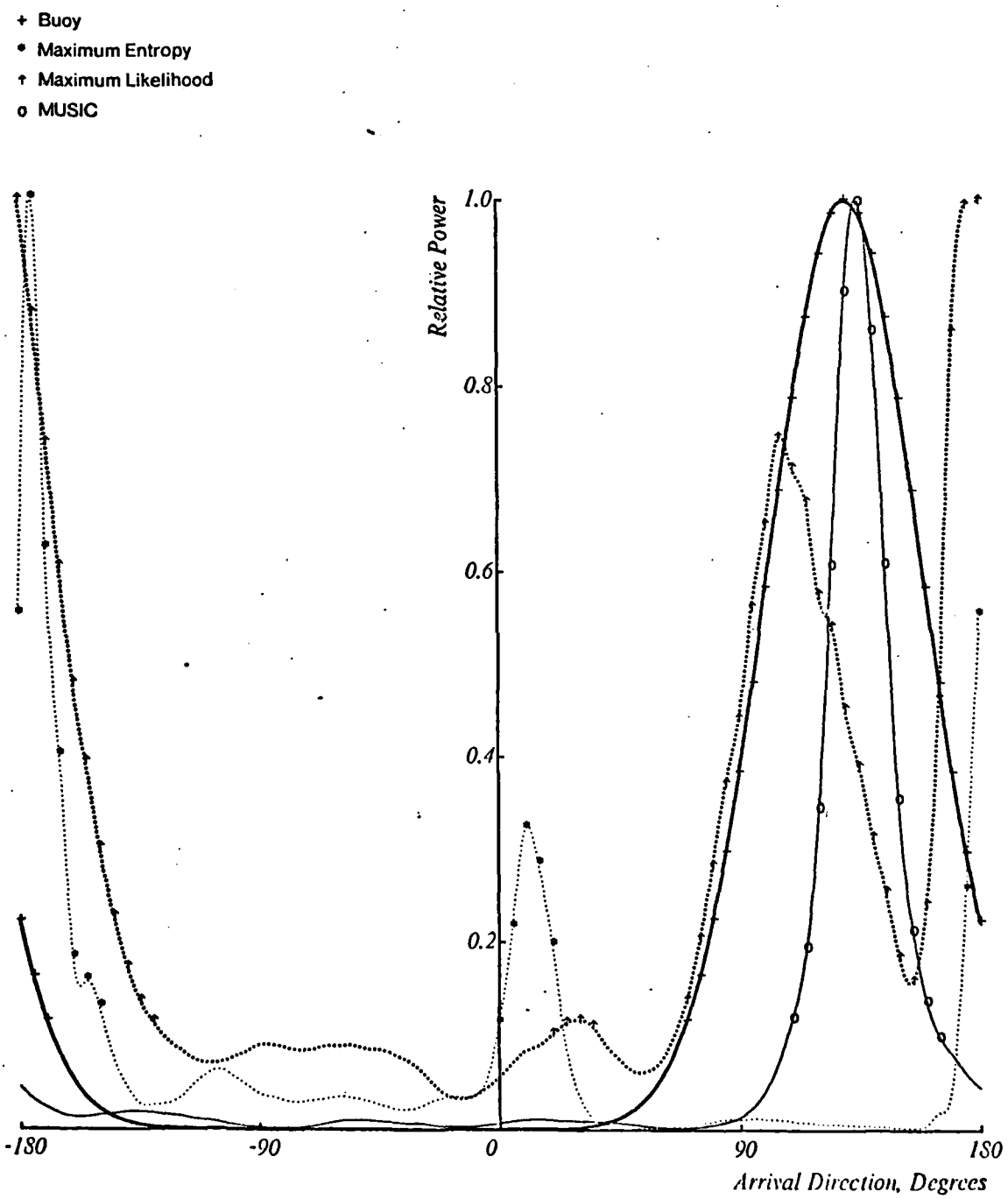

Figure 18

Buoy, ME, ML, and MUSIC spectrum estimators. 5 Sept. 78, 6.78 MHz. The vertical scale is linear in relative power. The x-axis represents degrees True.

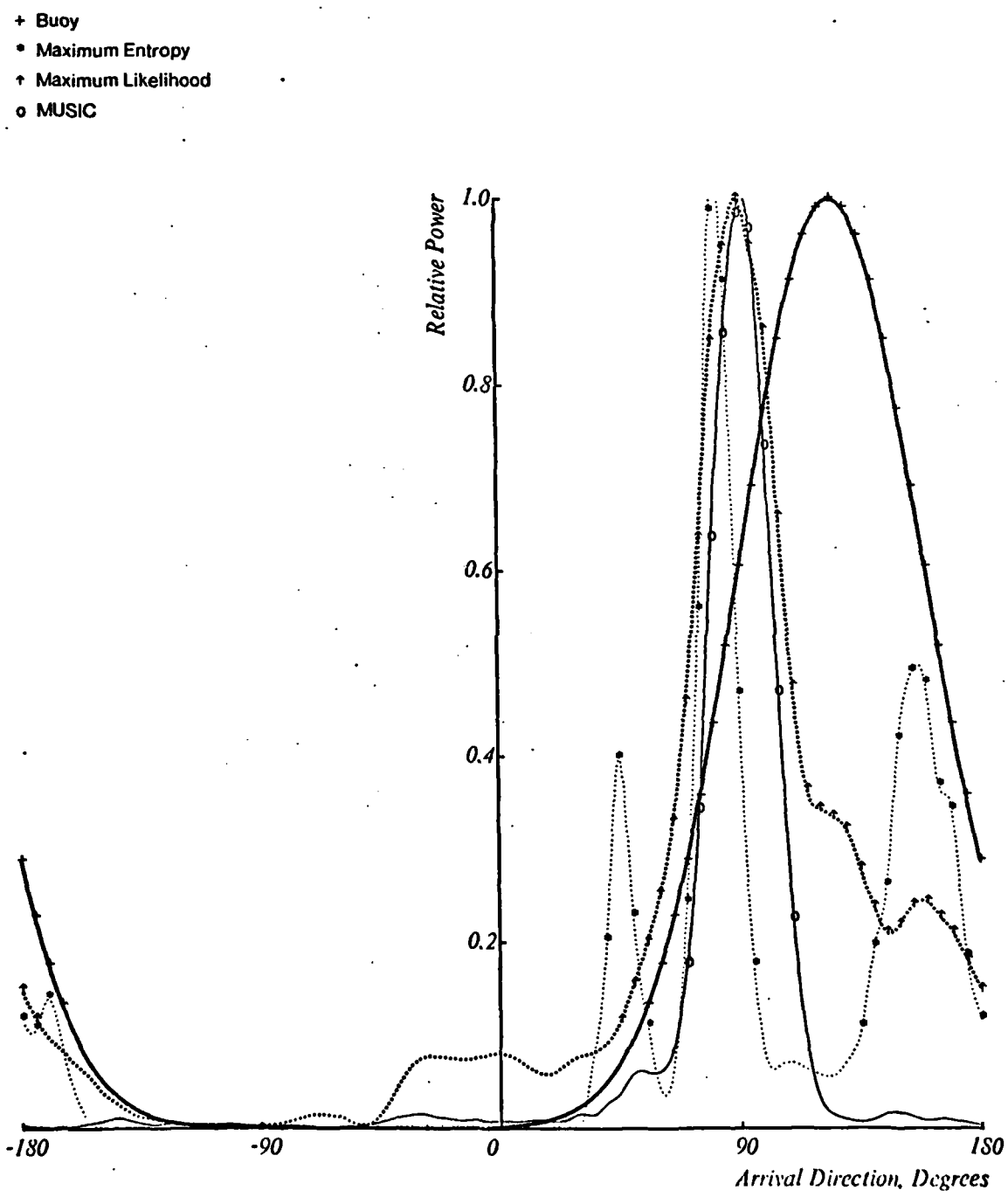

Figure 19

Buoy, ME, ML, and MUSIC spectrum estimators. 5 Sept. 78, 13.38 MHz. The vertical scale is linear in relative power. The x-axis represents degrees True.

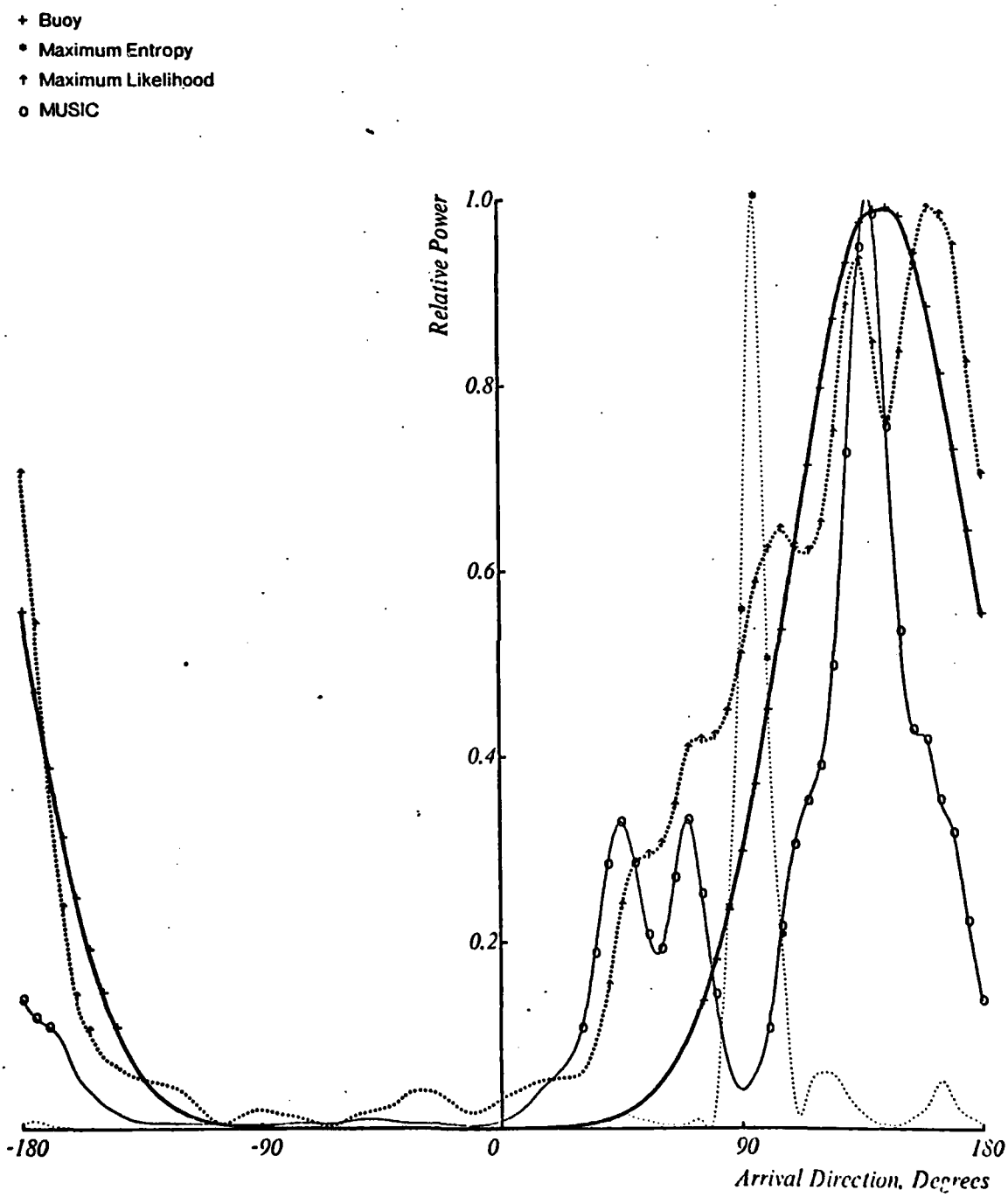

Figure 20

Buoy, ME, ML, and MUSIC spectrum estimators. 5 Sept. 78, 21.77 MHz. The vertical scale is linear in relative power. The x-axis represents degrees True.

4.80 MHz					
Method	N_{01}	N_{10}	N_{02}	N_{20}	N_{11}
Buoy	0.666	−0.335	0.758	0.432	−0.104
MUSIC	0.507	−0.528	0.475	0.526	−0.212
ML	−0.141	−0.393	0.178	0.822	−0.024
ME	−0.571	0.641	0.377	0.623	−0.382

6.78 MHz					
Method	N_{01}	N_{10}	N_{02}	N_{20}	N_{11}
Buoy	0.583	−0.586	0.607	0.648	−0.237
MUSIC	0.602	−0.650	0.481	0.519	−0.395
ML	0.272	−0.460	0.454	0.546	−0.062
ME	−0.144	0.339	0.171	0.829	0.117

13.38 MHz					
Method	N_{01}	N_{10}	N_{02}	N_{20}	N_{11}
Buoy	0.436	−0.529	0.813	1.030	0.039
MUSIC	0.800	−0.010	0.798	0.202	0.001
ML	0.705	−0.110	0.683	0.316	−0.055
ME	0.667	0.238	0.571	0.429	−0.007

21.77 MHz					
Method	N_{01}	N_{10}	N_{02}	N_{20}	N_{11}
Buoy	0.308	−0.421	0.568	0.714	0.068
MUSIC	0.601	−0.386	0.476	0.524	−0.164
ML	0.530	−0.469	0.472	0.528	−0.147
ME	0.933	−0.150	0.904	0.095	−0.104

Table 2

Comparison of moments, 5 Sept. 1978. Wind speed 12.3 m s^{-1} from 120°T.

inspection of the smoothed radar frequency spectra). A linear regression analysis was applied individually to these remaining shear values as a function of the shear predicted by (9) for the waves and that predicted by (8) for the wind, and finally a multiple linear regression analysis was performed against both the wind- and wave-predicted shears.

Summary of Measured and Predicted Shears – JASIN				
Date, 1978	Radar meas.	Total est.	Wind est.	Wave est.
4 Aug	6.8	2.98	1.34	1.64
5 Aug	7.2	4.72	1.91	2.81
6 Aug	8.0	6.80	3.20	3.60
7 Aug	3.7	5.35	2.34	3.01
7 Aug	3.9	5.35	2.34	3.01
8 Aug	3.8	3.38	1.79	1.59
8 Aug	2.5	3.40	1.80	1.60
10 Aug	5.8	7.19	3.50	3.69
11 Aug	7.6	7.88	3.87	4.01
11 Aug	8.3	7.88	3.87	4.01
13 Aug	6.8	8.13	3.57	4.56
13 Aug	8.2	8.13	3.57	4.56
14 Aug	4.4	3.18	1.72	1.46
24 Aug	6.0	7.43	3.87	3.56
25 Aug	5.0	4.60	2.73	1.87
25 Aug	8.6	4.60	2.73	1.87
25 Aug	5.3	4.60	2.73	1.87
28 Aug	5.7	6.87	3.40	3.47
31 Aug	8.6	6.61	3.51	3.10
31 Aug	3.2	6.61	3.51	3.10
1 Sep	6.2	5.74	2.96	2.78
1 Sep	7.2	5.74	2.96	2.78
5 Sep	11.7	11.29	5.68	5.61
5 Sep	12.8	10.71	5.37	5.34

Table 3

Summary of JASIN radar measurements and wind- and wave-predicted values for the current shear. The radar values represent the difference in $\mathrm{cm\,s^{-1}}$ between the current velocities obtained from radar measurements of 6.9 m and 31.2 m ocean wave phase velocities. The wind and wave estimates of the shear are based on the difference in current velocities predicted for depths of 30 cm and 137 cm, respectively. These are the depths at which the 6.9 m and 31.2 m waves are coupled to the currents, assuming a logarithmic current profile.

5.2.2 Estimating the ocean-wave directional spectrum

In a recent Ph.D. thesis, *Elabdalla* [1982] examined the use of several super-resolution spectral estimation techniques to estimate the ocean-wave directional spectrum,

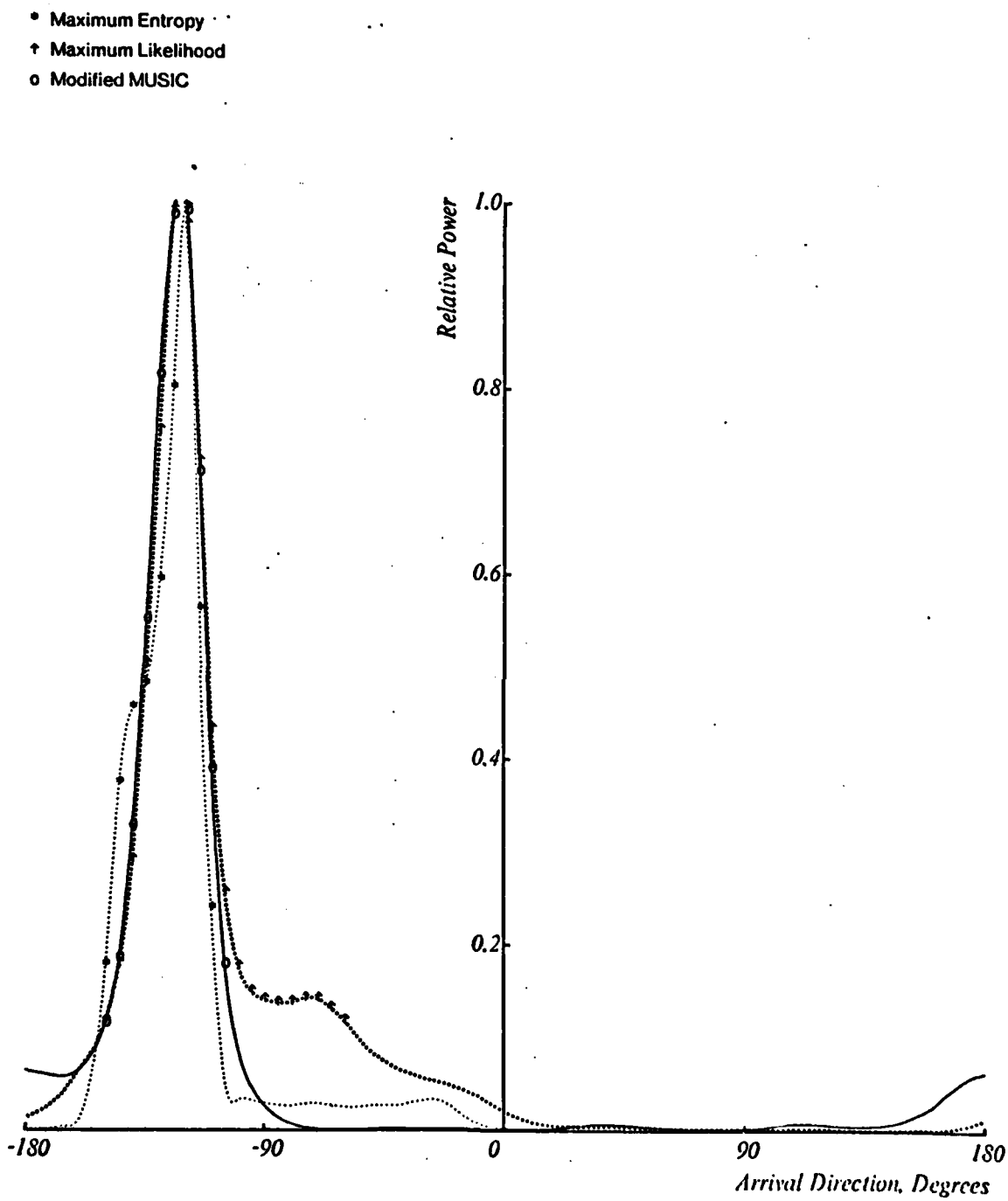

Figure 21

Comparison of ME, ML, and MUSIC spectrum estimators. This figure illustrates the improvement using the modified MUSIC algorithm as compared to the ML and ME altorighms. Data were collected from a beacon transponder located at −125°. The vertical axis is linear in relative power.

and he applied these techniques to the JASIN HF radar data. These techniques, normally used to estimate a frequency spectrum from a set of time samples, were used to estimate the ocean-wave directional spectrum from a set of spatial samples at the positions of the receiving loops on the R.V. *Atlantis-II*. He compared results obtained using the MUltiple Signal Classification (MUSIC), Maximum Entropy (ME), and Maximum Liklihood (ML) estimators against the directional spectrum estimates from the pitch-roll buoy and synthetic aperture radar (SAR) processing of some of the JASIN data.

In order to demonstrate the directional resolution of the different techniques, the directional spectrum of a calibration beacon on the R.V. *Meteor* was estimated. Ideally this should be a delta function. Figure 21 illustrates the results of this test. The MUSIC algorithm provided an unbiased estimate of the directional spectrum, while the ML and ME algorithms provided somewhat biased estimates. All three altorighms correctly identified the direction of the beacon.

The algorithms were used to estimate the ocean-wave directional spectrum under moderate wind conditions (12 $\mathrm{m\,s^{-1}}$) on 5 September 1978. Figures 17–20 show the results of these algorithms as well as the estimates provided by the pitch-roll buoy. Again, the MUSIC algorithm gave results which agreed best with the buoy estimates. Table 2 compares the first five moments N_{pq} for the various algorithms. N_{pq} is defined by

$$N_{pq} = \frac{\int_0^{2\pi} P(k,\theta) cos^p(\theta) sin^q(\theta)\, d\theta}{\int_0^{2\pi} P(k,\theta)\, d\theta} \tag{12}$$

where $P(k,\theta)$ is the ocean-wave directional spectrum estimate for ocean wavenumber k and direction θ, and p and q range from 0 to 2. Again, the moments calculated with the MUSIC algorithm were closest to the buoy moments. Further details can be found in [*Elabdalla*, 1982].

5.3 Results

The results of the JASIN experiment are summarized in Table 3 and are indicated

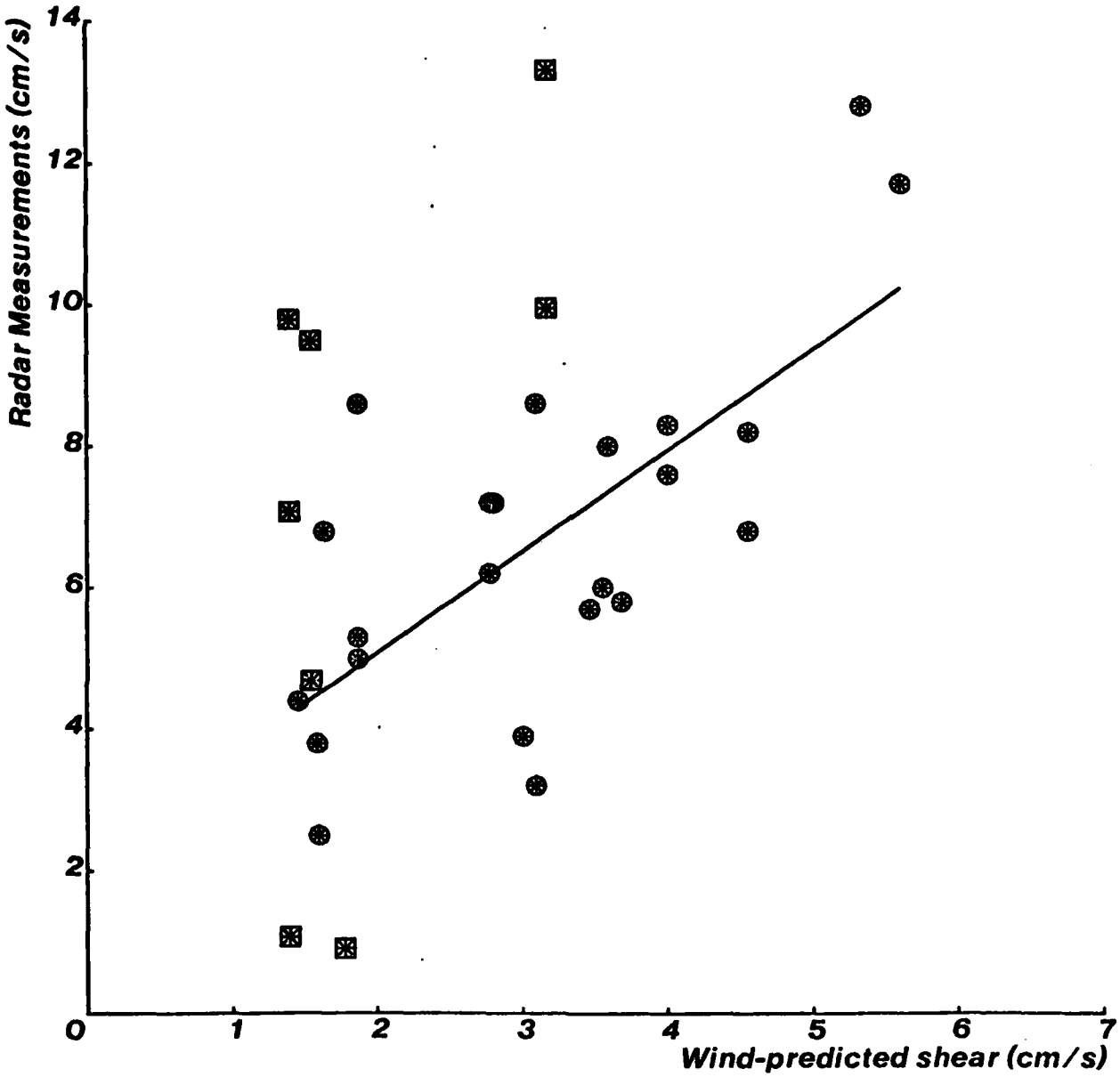

Figure 22

The radar-measured shear *vs.* the shear predicted by the wind alone. The radar shear is the difference in the deviations of the phase velocities from their still-waver values for the 6.9 m and 31.2 m ocean waves, averaged over all range bins. The squares indicate measurements obtained by *Ha* along the California coast in January 1978. The velocity is the difference in current velocity at depths of 30 cm and 137 cm. These are the depths at which the 6.9 m and 31.2 m ocean waves are effectively coupled to the currents if the current distribution is logarithmic with depth. From eq. (6), these can be converted to u_{*water} by dividing by 3.78.

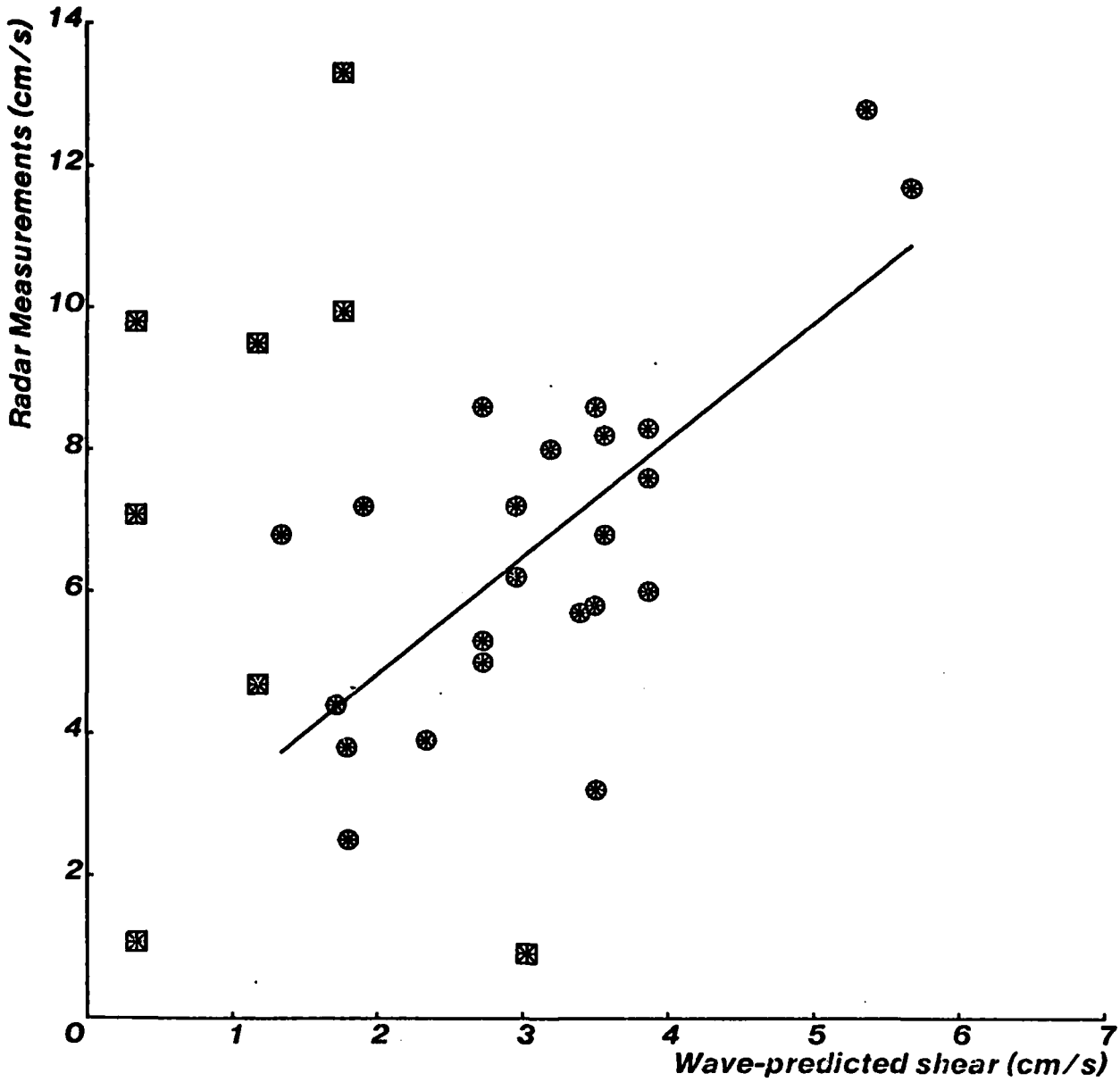

Figure 23
The radar-measured shear *vs.* the shear predicted by the waves alone. The velocities are as in Fig. 22.

graphically in Figures 22–24. As in the Pescadero experiments, the estimate of the wind- and wave-generated current shear was made with the assumption of a logarithmic current profile.

The wind velocity during JASIN was generally low, reaching 10 $m s^{-1}$ on only

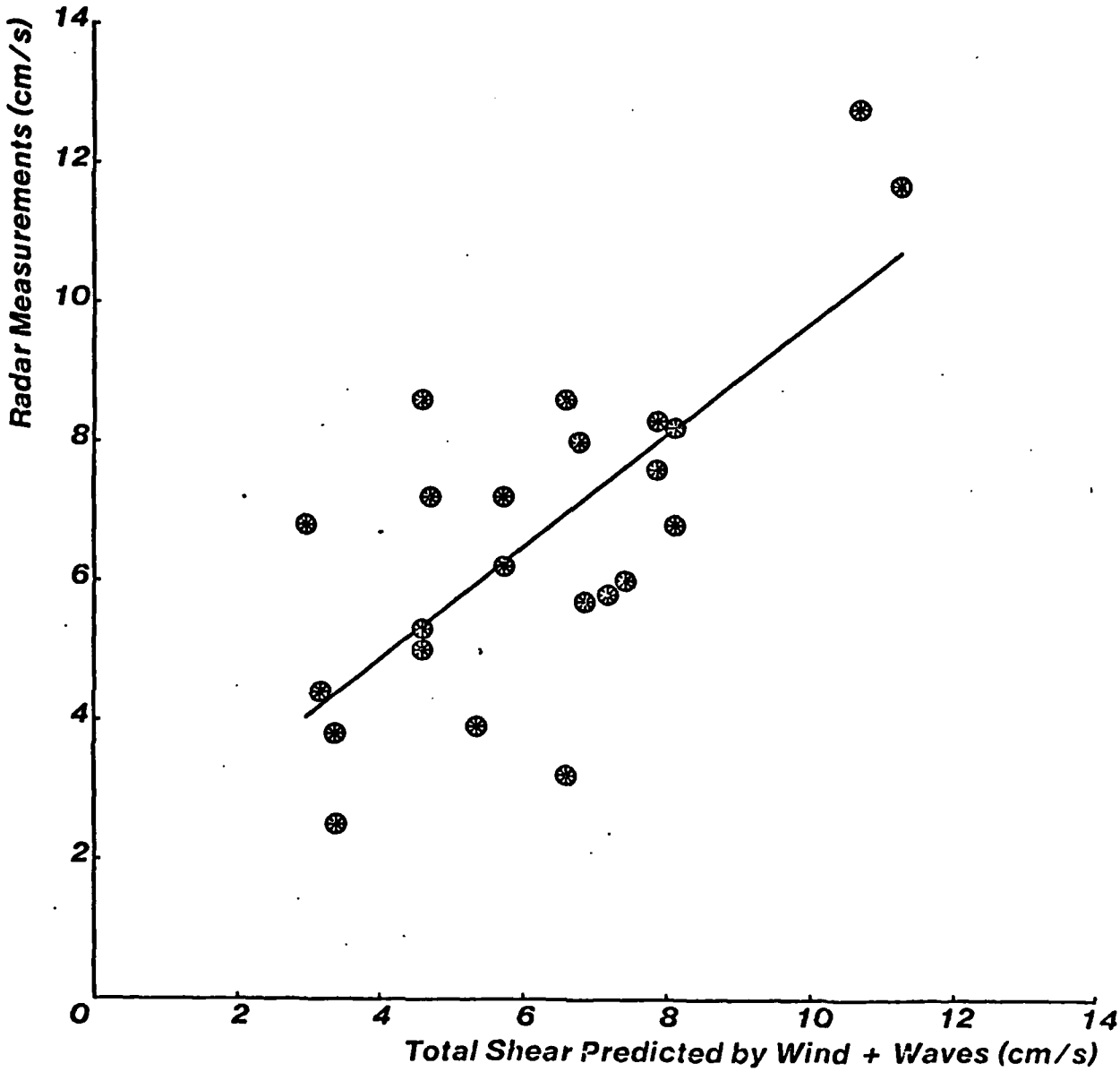

Figure 24
The radar-measured shear *vs.* the shear predicted by the sum of the wind- and wave-induced components, assuming that they are colinear. The velocities are as in Fig. 22.

two or three occasions. The wave heights were correspondingly small. Under these conditions, the expected shear generated by the wind and the waves are nearly identical, as indicated in Table 3. The radar measurements indicated vertical shears larger than

predicted by either the wind alone (Figure 22) or the waves alone (Figure 23), but somewhat less than would be expected if the wind- and wave-induced components were assumed colinear and added together (Figure 24). For this data set, the single-variable regression on the waves alone resulted in a slightly higher correlation coefficient than the single-variable regression on the wind alone (0.71 vs. 0.70), although the difference is probably not significant. The two-variable regression on both the wave- and wind-induced shears was slightly better, resulting in a correlation coefficient of 0.72, with the regression equation

$$u_{*radar} = (1.05 \pm 0.80)u_{*waves} + (0.59 \pm 0.71)u_{*wind} + (1.54 \pm 1.18) \qquad (13)$$

where u_{*radar} is calculated from the radar-measured shear through (6), u_{*wind} is estimated from (8), and u_{*waves} is estimated from (9), (3)and (6). The standard errors are based on a 10% risk level.

Chapter 6

Summary and Conclusions

The Pescadero experiments demonstrated that a current could be measured by an HF radar, and that its value agreed reasonably well with that measured by *in-situ* drifting spar buoys. In addition, there was evidence of a vertical current shear, both from the radar measurements and from the buoy measurements. The design of the equipment was proven and the data processing techniques were developed in the Pescadero experiments.

The JASIN experiment was an attempt to apply the techniques developed in the Pescadero experiments to the measurement of surface current and current shear in the open ocean. The radar system offered the possiblity of making a measurement that no other instrument could make. The radar was successfully installed and operated on board a ship with tolerable interference to the normal shipboard activities. The steerable antenna proved to be quite rugged and successful. The antenna patterns which were achieved were what would be expected from the physical aperture of the receiving array.

The wind velocity during all of the JASIN experiment, except during the period when the ship was in port, was much lower than had been expected, so wind- and wave-generated currents were quite small. Nevertheless, there is some evidence of a current shear. Its magnitude is small, however, and it is near the resolution limit of the radar system. There were many steps involved in the data processing, including the Fourier processing of the radar echo signal, the formation of a narrow antenna beam in several

different directions at each radar frequency, and the estimation of the Doppler shift of the radar echo by the estimation of four parameters of a model for the ocean directional spectrum (center and width) and relative motion between ship and water (magnitude and direction). Consequently, it is very difficult to compute the overall precision of the radar measurements. The internal consistency of the radar measurements from one range cell to the next suggests a figure of about $5\,\mathrm{cm\,s^{-1}}$. Although the two-variable regresssion indicates that the wave-induced component of shear may have a slightly higher correlation with the radar measurements than the wind-induced component (and this was also the case when individual range bins were processed separately), this may be the result of noisy data. However, the radar measurements indicate a shear higher than would be expected from either component alone. *Ha* also noted that the shear he measured at Pescadero gave a value about twice that predicted from the wind alone (Figure 10).

References

Barrick, D. E.: 1971, "Dependence of second-order sidebands in HF sea echo upon sea state", *IEEE G-AP International Symposium Digest*, Sept. 21-24, Los Angeles, California, 194–197.

Barrick, D. E.: 1972a, "First-order theory and analysis of MF/HF/VHF scatter from the sea", *IEEE Transactions on Antennas and Propagation*, AP-**20**, 2–10.

Barrick, D. E.: 1972b, "Remote sensing of sea state by radar", in *Remote Sensing of the Troposphere*, V. E. Derr (ed.), Ch. 12, U. S. Government Printing Office, Washington, D.C.

Barrick, D. E., M. W. Evans and B. L. Weber: 1977, "Ocean surface currents mapped by radar", *Science* **198** (14 Oct. 1977), 138–144.

Crombie, D. D.: 1955, "Doppler spectrum of sea echo at 13.56 Mc/s", *Nature* **175**, 681–682.

Elabdalla, Abdelrahman M.: 1982, "Remote sensing of the directional ocean wave spectra using HF backscatter radar", Ph.D. dissertation, Stanford University.

Ha, E. C.: 1979, "Remote sensing of ocean surface current and current shear by HF backscatter radar", Ph.D. dissertation, Stanford University, Stanford Electronics Laboratories Technical Report D415-1, August 1979.

Hasselmann, K.: 1966, "Feynman diagrams and interaction rules of wave-wave scattering processes", *Review of Geophysics*, **4**, 1–32.

Hasselmann, K.: 1971, "Determination of ocean wave spectra from Doppler radio return from the sea surface", *Nature, Physical Sciences*, **229**, 16–17.

Kenyon, Kern E.: 1969, "Stokes Drift for Random Gravity Waves", *Journal of Geophysical Research* **74**, 28, 6991–6994.

Kinsman, Blair: 1965, *Wind Waves*. Prentice Hall, Inc., Englewood Cliffs, New Jersey.

Stewart, R. H.: 1977, "A discus-hulled wave measuring buoy", *Ocean Engineering* **4**, 101–107.

Stewart, R. H. and J. W. Joy: 1974, "HF radio measurement of surface currents", *Deep-Sea Research* **21**, 1039–1049.

Teague, C. C., G. L. Tyler and R. H. Stewart: 1977, "Studies of the sea using HF radio scatter", *IEEE Transactions on Antennas and Propagation* **AP-25**, 12–19.

Tyler, G. L., C. C. Teague, R. H. Stewart, A. M. Peterson, W. H. Munk and J. W. Joy: 1974, "Wave directional spectra from synthetic aperture observations of radio scatter", *Deep-Sea Research* **21**, 989–1016.

Ursell: 1949, *Monthly Notices of the Royal Astronomical Society*, Geophysical Supplement.

Wu, Jin: 1975, "Wind-induced drift currents", *J. Fluid Mech.* **68**, part 1, 49–70.

Van Dyke, M. D.: 1982, *An Album of Fluid Motion*. The Parabolic Press, Stanford, California.